

---

[All ETDs from UAB](#)

[UAB Theses & Dissertations](#)

---

2023

## Alternating Current Electrospinning and Characterization of Nanofibrous Fish Skin Gelatin as an Innovative Biomaterial Platform

Amanda Kennell  
*University Of Alabama At Birmingham*

Follow this and additional works at: <https://digitalcommons.library.uab.edu/etd-collection>

 Part of the [Arts and Humanities Commons](#)

---

### Recommended Citation

Kennell, Amanda, "Alternating Current Electrospinning and Characterization of Nanofibrous Fish Skin Gelatin as an Innovative Biomaterial Platform" (2023). *All ETDs from UAB*. 423.  
<https://digitalcommons.library.uab.edu/etd-collection/423>

This content has been accepted for inclusion by an authorized administrator of the UAB Digital Commons, and is provided as a free open access item. All inquiries regarding this item or the UAB Digital Commons should be directed to the [UAB Libraries Office of Scholarly Communication](#).

ALTERNATING CURRENT ELELCTROSPINNING AND CHARACTERIZATION  
OF NANOFIBROUS FISH SKIN GELATIN AS AN INNOVATIVE BIOMATERIAL  
PLATFORM

by

AMANDA KENNEL

ANDREI STANISHEVSKY, COMMITTEE CHAIR  
NAMASIVAYAM AMBALAVANAN  
CHENG-CHIEN CHEN  
ALEN EBERHARDT  
RYOICHI KAWAI  
SERGEY VYAZOVKIN

A DISSERTATION

Submitted to the graduate faculty of The University of Alabama at Birmingham,  
in partial fulfillment of the requirements for the degree of  
Doctor of Philosophy

BIRMINGHAM, ALABAMA

2023

Copyright by  
Amanda Kennell  
2023

# ALTERNATING CURRENT ELELCTROSPINNING AND CHARACTERIZATION OF NANOFIBROUS FISH SKIN GELATIN AS AN INNOVATIVE BIOMATERIAL PLATFORM

AMANDA KENNEL

PHYSICS

ABSTRACT

A biomaterial for tissue repair is globally sought after, as transplant surgeries and general wound healing have a strong need for a manufactured scaffold that mimics the natural body's tissue in morphology, composition, and properties. This research presents a nanofibrous (NF) fish skin gelatin-based (FSG) substrate fabricated through an uncommon high-yield method of Alternating Current electrospinning that mimics that can mimic the natural body's extracellular matrix (ECM). An ECM is the first step in tissue repair. Fabrication through electrospinning gave the NF FSG substrate an identical mimic of the natural body's extracellular matrix morphology with nanofiber diameter on the order of  $175 \pm 19\text{nm}$  as spun. This nanofibrous FSG substrate is biocompatible having 10.2% cell confluence after 72 hours in a physiological environment. Additionally, it is bioactive as gelatin and other incorporated polysaccharides provide nutrients for wound repair. The FSG ECM is biomechanically viable as the stress-strain curve follows that of natural body tissue while the elastic moduli with post processing treatments in dry condition was  $11.4 \pm \text{MPa}$  and in wet conditions  $35.1 \pm 7.2\text{kPa}$ . The fabrication method of electrospinning is scale-up making the FSG ECM mass producible with a production rate of 12.6g/h. This nanofibrous FSG substrate is an innovative biomaterial platform as it retains ideal biomaterial properties of biocompatibility, bioactiveness, biomechanically viable, and mass-producible.

Keywords: Fish Skin Gelatin, Alternating Field Electrospinning, Nanofibers, Extracellular Matrix, Viscoelastic, Crosslink

## DEDICATION

To my parents, Tim and Joyce Kennell, and brother, Timothy Kennell

## ACKNOWLEDGMENTS

To my mentors I would express my sincere gratitude for their incredible amount of time and guidance throughout my PhD journey. Specifically, I would like to thank Andrei Stanishevsky. He has been a great mentor to me and strong advocate of my professional development. The opportunities he provided me with and encouraged me to go after is the reason I am where I am today. Additionally, I would like to thank each of my committee members. For the time and help they provided me with to be multifaceted in my approaches for any research investigation.

To my family I am deeply grateful for their unwavering belief and support in me through my long journey. My mother, Joyce, who dedicated thirteen years of her life homeschooling me and instilling in me a strong drive and love for learning. My father, Tim, who always encouraged me to never do less than my best and was a pillar of support for me to lean on. My brother, Timothy, who stayed up many late nights listening to my research speeches and projects. He always provided me with invaluable feedback and help. After, of course, teasing me for conspicuous mistakes that we both laughed at.

## TABLE OF CONTENTS

|  | Page |
|--|------|
| ABSTRACT.....  | iii  |
| DEDICATION.....  | v    |
| ACKNOWLEDGMENTS .....  | vi   |
| LIST OF TABLES.....  | viii |
| LIST OF FIGURES .....  | x    |
| LIST OF ABBREVIATIONS.....   | xiv  |
| CHAPTER  |      |
| 1. INTRODUCTION .....  | 1    |
| 1.1 History of Tissue Engineering .....  | 2    |
| 1.2 The Backbone of Biomaterial .....  | 7    |
| 1.3 biomechanical Properties of the Extracellular Matrix .....   | 8    |
| 1.4 Mass-producible fabrication .....  | 11   |
| 1.5 Hypothesis and Aims .....  | 13   |
| 2. FISH SKIN GELATIN NANOFIBROUS SCAFFOLDS SPUN USING<br>ALTERNATING FIELD ELECTROSPINNING AND <i>IN-VITRO</i><br>TESTED WITH TDTOMATO MICE FIBROBLASTS..... | 16   |
| 3. DEGRADATION BEHAVIOR AND VISCOELASTIC PROPERTIES<br>OF ELECTROSPUN FISH SKIN GELATIN-BASED NANOFIBROUS<br>SUBSTRATE IN BIOLOGICAL ENVIRONMENT.....        | 58   |
| 4. CONCLUSION.....   | 93   |
| LIST OF REFERENCES.....  | 95   |

## LIST OF TABLES

| Table  |  | Page |
|--|--|------|
| <b>FISH SKIN GELATIN NANOFIBROUS SCAFFOLDS SPUN USING<br/>ALTERNATING FIELD ELECTROSPINNING AND IN-VITRO TESTED WITH<br/>TDTOMATO MICE FIBROBLASTS</b> |  |      |
| 1  | Table 1. Precursor compositions for pure FSG nanofiber with varying amounts of AA.....   | 57   |
| 2  | Table 2. Precursor compositions of FSG nanofibers with varying amounts of varying amounts of cmCEL.....  | 57   |
| 3  | Table 3. Young’s moduli of fish gelatin based nanofibrous scaffolds tested under tensile load after the exposure in SBF for 1 and 3 days.....  | 57   |
| <b>DEGRADATION BEHAVIOR AND VISCOELASTIC PROPERTIES OF<br/>ELECTROSPUN FISH SKIN GELATIN-BASED NANOFIBROUS SUBSTRATE<br/>IN BIOLOGICAL ENVIRONMENT</b> |  |      |
| 1  | Table 1. Composition of fGel precursors without and with additives CMC (fCMC) and chitosan (fChi). .....   | 66   |
| 2  | Table 2. Post-processing procedures for fGel-based nanofibrous materials. Thermal crosslinking (T) was used in every case and freeze-drying (F) was use in the half of the tests. Letter G indicates glutaraldehyde crosslinking and letter A indicates glucosamine enhanced thermal crosslinking. ....  | 68   |
| 3  | Table 3: Elasticity moduli of fCMC, fChi, and fGel after crosslinking with FTA and FTG. The material was strained when dry, after five minutes of exposure to FBS, and after degrading in FBS for 24 hours. The crosslinking procedure FTA performed best for the dry material. For the wet material fChi became stiffer after 24hours in FBS fGel and fCel did not have significant change when wet. .... | 78   |

|   |  |    |
|---|--|----|
| 4 | Table 4: Porosity of each material with various crosslinking procedures. The porosity was very similar. .... | 79 |
|---|--|----|

## LIST OF FIGURES

Figure Page

### INTRODUCTION

- 1 Figure 1: polymer scaffold made through photolithography. (a) is the light source that strikes (b) a photoresist material that only allows selected regions of light to pass through. (c) is the silicon mold that is being etched on. (d) is the polymer solution that will be hardened into a scaffold. ....3
- 2 Figure 2: DC electrospinning a nanofiber. (a) is the power supply connected to the (b) syringe which projects a polymer solution forward to the oppositely charged collector.....6
- 3 Figure 3: example of an ECM with random fiber morphology. ....7
- 4 Figure 4: (a) is stress-strain curve for normal body tissue. (a.i) is the toe region (a.ii) is the elastic region (a.iii) is the plastic regions (a.iv) is the failure region where the samples breaks. 3.b shows the nanofibers orientation as they are being strained.....9
- 5 Figure 5: AC electrospinning FSG nanofibers. (a) adapted from Kennell et al [34] showing the FSG solution on the electrode before an  $\nabla E$  is created. (b) shows the production of nanofibers after the electrohydrodynamic process starts.....12

### FISH SKIN GELATIN NANOFIBROUS SCAFFOLDS SPUN USING ALTERNATING FIELD ELECTROSPINNING AND IN-VITRO TESTED WITH TDTOMATO MICE FIBROBLASTS

- 1 Figure 1. Process of creating and in-vitro testing the FSG biomaterial. (a) The FSG precursor has a consistency of syrup. (b) The AFES process, (iv) electrode that the (iii) FSG precursor is placed on. After creating a potential difference in the FSG precursor (ii) nanofibers are lifted by ionic winds and initial impulse of the created fibers to the (i) collector which rotates collecting sheets of (c) nanofibers. (c.i.) A similar morphology to the ECM can be seen with an SEM image. (d) After confirmation, the nanofibers thermally crosslinked in an oven. After sterilization (e) in-vitro seeding of tdTomato fibroblasts confirms that the FSG is a viable biomaterial with (e.i.) cell growth. ....48

|   |  |    |
|---|--|----|
| 2 | Figure 2. SEM images and distribution of nanofiber diameters before thermal crosslinking and after thermal crosslinking. Before thermal crosslinking are (a) FSG (b) FSGAA-10 (c) FSGAA-5 (d) FSG/CEL-5. Histogram of uniform nanofiber diameters after thermal crosslinking where visible shrinkage in fiber diameter can be observed by the peaks shifting left. A side effect of thermal crosslinking was causing more uniform fiber diameters seen by the peak being skewed to the middle (e) FSG (f) FSGAA-10 (g) FSGAA-5 (h) FSG/CEL-5. .... | 49 |
| 3 | Figure 3. Fig. 3. Average fiber diameters of the different scaffolds comparing noncrosslinked to thermally crosslinked scaffolds. FSG, FSGAA-5, FSG/CEL-5 nanofiber diameters all shrank axially, while FSGAA-10 indicated a lateral increase in fiber diameters. ....   | 50 |
| 4 | Density histograms of the nanofiber sheets showing a uniform distribution over different cross sections of the sheet. The peak of each histogram normally lies at the same density except for (a) FSG nanofiber which indicate a higher density for crosslinking at 160 °C for 8h due to FSG non-Newtonians nature. The other nanofiber sheets (b) FSGAA-10 (c) FSGAA-5 and (d) FSG/ CEL show a normal distribution for all crosslinking procedures around the same density.....   | 51 |
| 5 | Percent of mass retained of the whole scaffold for varying thermal crosslinking procedures. The nanofiber scaffolds were thermal crosslinked at (a) 180 °C for 4h (b) 160 °C for 4h and (c) 160 °C for 8h. The samples thermally crosslinked at 160 °C for 8h retained the most mass, and the addition of cmCEL made the nanofiber scaffold retain even more mass then the pure FSG nano-fiber scaffold. ....  | 52 |
| 6 | (a) FTIR Spectrum comparing the molecular structure before crosslinking, after crosslinking, and after sterilization. There is some oxidation in the band region around 1700 cm-1 after UV sterilization. The degradation is small and not concerning. (b) FTIR Spectrum comparing the molecular structure between the varying nanofiber composition in Tables 1 and 2. All spectra show the same trend except FSG/CEL 5 and 10 have a cellulose band in the 1000 cm-1 region. ....  | 53 |
| 7 | Proliferation and healthy cell growth across the varying scaffolds from Tables 1 and 2. (a) The scaffolds with 0.5% cmCEL had the largest confluence. (b) the FSGAA-5 scaffold showed a higher cell confluence. This scaffold held the same nanofiber composition as the FSG/CEL-5 without the additional 0.5% cmCEL (c) These 5% cmCEL scaffolds had the largest area of cells (d) compared to the FSGAA-5. ....  | 54 |
| 8 | (a) Fluorescence images of fixed tdTomato fibroblasts proliferation across the varying ECM compositions: (a.i.) FSG  |    |

(a.ii.) FSG/CEL-5 (a.iii.) FSG/CEL-1 (a.iv.) FSGAA-5 (a.v.) FSGAA-10 (a.vi.) FSGAA-15. The difference in the cell proliferation between the ECM with cmCEL compared to those without can strongly be seen between (a.iii.) and (a.vi.). (b) Fluorescence images of live TdTomato fibroblasts proliferation across the varying ECM compositions: (b.i.) FSG (b.ii.) FSG/CEL-5 (b. iii.) FSG/CEL-1 (b.iv.) FSGAA-5 (b.v.) FSGAA-10 (b.vi.) FSGAA-15. The individual nanofiber strands with cells proliferating across the ECM can be seen best in (b.ii.) and (b.iv.). .....55

9 (a) Composite fluorescence image of (i) FSG/Cell-1 ECM in comparison with only(ii) GFP fluorescence and (iii) tdTomato natural fluorescence of the fi broblasts; (b) Composite fluorescence image at  $\times 400$  of(i) FSGAA-5 ECM in comparison with only (ii) the GFP fluorescence of the cell's actin and (iii) the tdTomato fluorescence of the mitochondrial. ....56

**DEGRADATION BEHAVIOR AND VISCOELASTIC PROPERTIES OF ELECTROSPUN FISH SKIN GELATIN-BASED NANOFIBROUS SUBSTRATES IN BIOLOGICAL ENVIRONMENT**

1 Figure 1. FSG NFs produced by AFES then crosslinked various ways to mimic a biomaterial's mechanical properties. (a) is FSG NFs being fabricated with a cylindrical shape. (b) is the fGel material thermally crosslinked with and without AGA enhancement. AGA causes the color change in the fGel NFs material due to the Maillard during thermal crosslinking. (c) is fGel material prepared for a degradation test. (d) shows the fGel material after the degradation test being dried in a vacuum. (e) is fGel material cut and placed into frames. The frames prevent the NFs from folding while in SBF. (f) is mechanically testing dry fGel material. (g) is before straining and after breaking the dry fGel material. (h) is fGel material being strained in FBS at  $37^{\circ} C$ . .....87

2 Figure 2. Mass loss of fGel material with various crosslinking methods. The fGel-FTG and fGel-FTA degraded the least losing 10.7% (FTG) and 15.0% (FTA) of their original mass after a week period. Comparatively the fGel-T material lost the most mass over the week period. If T crosslinking was combined with another post-processing method the material retained more mass. ....88

3 Figure 3 FTIR absorption spectra fGel NF materials initially after (a) electrospinning and thermal crosslinking, (b) then after 1 day and (c) then 7 days of degradation in SBF.....89

4 Figure 4. Stress vs. Strain curves of fGel, fCMC, and fChi materials. (a.i.) shows non-crosslinked Gel material's

mechanical behavior. (a.ii.) shows non-crosslinked fCMC material's mechanical behavior, additionally, with the four regions of a stress vs. strain curve with NF morphology changing as the material is strained. fCMC reaches the highest stress level. (a.iii.) shows non-crosslinked fChi material. (b.i.) shows fGel-FTA crosslinked material's mechanical behavior while dry. (b.ii.) shows fCMC-FTA crosslinked material's mechanical behavior while dry. (b.iii.) shows fChi-FTA crosslinked materials mechanical behavior while dry. ....90

5 Figure 5: tensile tests of various gelatin materials crosslinked different ways. (a) materials were strained laterally to obtain there elasticity modulus and yield strength. The fCMC material regardless of crosslinking procedure had the highest elasticity modulus. (b) is the maximum stress withstood by the FSG material until breakage. The fCMC material withstood the highest stress. ....91

6 Figure 6: fCMC material mechanically tested in a physiological environment. The material is in FBS at a temperature of 37°C. (a.i.) is fCMC-FTA crosslinked and (b.i.) is fCMC-FTG crosslinked both have been just submersed in SBF for 5min. (a.ii.) is fCMC-FTA crosslinked and (b.ii.) is fCMC-FTG crosslinked both have been left in FBS at normal body temperature for twenty-four hours. Some materials never broke as they were too elastic. The elastic modulus was taken from the second elastic region. ....92

## LIST OF ABBREVIATIONS

|                   |   |
|-------------------|---|
| AA                | Acetic Acid                                 |
| AC                | Alternating current                         |
| AFES              | Alternating field electrospinning           |
| AGA               | N-Acetyl-D-glucosamine                      |
| ATR               | Attenuated Total Reflectance                |
| Chi               | chitosan                                    |
| CMC               | Carboxymethyl cellulose sodium salt         |
| cmCEL             | Carboxymethyl cellulose sodium salt         |
| C-Spin            | Centrifugal spinning                        |
| CTD               | computational topology design               |
| DC                | direct current                              |
| dH <sub>2</sub> O | deionized water                             |
| DPBS              | Dulbecco's phosphate buffer saline solution |
| ECM               | extracellular matrix                        |
| FBS               | fetal bovine serum                          |

|      |   |
|------|---|
| fChi | fish skin gelatin with chitosan material                            |
| fCMC | fish skin gelatin with Carboxymethyl cellulose sodium salt material |
| FD   | freeze dry  |
| FDM  | Fused deposition modeling   |
| fGel | fish skin gelatin material  |
| FSG  | fish skin gelatin   |
| FTA  | freeze dried N-Acetyl-D-glucosamine enhanced thermal                |
| FTG  | freeze dried thermal and glutaraldehyde vapor                       |
| FTIR | Fourier Transform Infrared spectroscopy                             |
| GFP  | green fluorescent protein   |
| GTA  | glutaraldehyde  |
| PCL  | Polycaprolactone  |
| PLA  | Polylactic acid   |
| PU   | Polyurethane  |
| IR   | infrared spectroscopy   |
| NFs  | nanofibers  |
| PBS  | phosphate buffer saline solution                                    |
| SBF  | synthetic body fluid  |
| SBS  | solution blow spinning  |
| SD   | standard deviation  |

|     |   |
|-----|---|
| SFF | Solid Free-form                         |
| SEM | scanning electron microscopy            |
| T   | thermal                                 |
| TA  | N-Acetyl-D-glucosamine enhanced thermal |
| TE  | tissue engineering                      |
| TG  | thermal and glutaraldehyde vapor        |

## INTRODUCTION

Tissue Engineering (TE) a material that mimics natural body tissue would have strong impacts in the medical field. During transplant surgeries, a doctor must utilize an organ from an organ donor or perform a second surgical procedure on the patient in order to obtain tissue. Having a natural biomaterial stock of manufactured tissue would eliminate time and need to wait for organ donors as well as prevent a second surgery for the patient. While the idea of TE biomaterial has been around for several centuries, it did not become popular until the 1990's. Before TE, organ donors were the only method of tissue replacement for transplant surgeries. However, due to patients' high rejection rate of the foreign tissue, many started seeking enhanced or alternative methods for replacement tissue.

In the 1980's, Doctors Burke and Green were the first two surgeons to TE and surgically implement a biodegradable matrix as skin into a burn patient [1]. This study was published in 1991, as one of the first papers to use the term tissue engineering. A few years later in 1988, Vacanti et al was one of the first groups to begin in-vivo-testing a TE biodegradable polymer matrix for immunological response [1]. In 2008, another surgical procedure occurred to replace a patient's trachea and became the first 3-dimensional organ to be tissue engineered. The trachea came from an organ donor, was decellularized and reseeded with cells then cultured until implementation [2]. As the tissue engineering field grew several key components for a TE material surfaced. The

material needed to be biocompatibility, bioactive, biomechanically viable, and mass-producible in order to have a low rejection rate from patients and not procure a harmful immunological response.

### 1.1 History of Tissue Engineering

For tissue regeneration and repair there are two ways to TE a scaffold. These are *in-situ* TE as in the case from Vacanti in 1988 when a scaffold was fabricated from polymers, and *ex-vivo* TE like the surgical trachea case in 2008. The trachea scaffold came from an organ donor's body tissue. While *ex-vivo* TE has been successfully implemented, there is a rejection rate concern for the foreign body tissue. Additionally, there can be a large wait time for right organ donor [2]. *In-situ* TE a scaffold is a good alternative to *ex-vivo* nullifying these concerns, however, manufactured scaffolds tend to have worse mechanical properties. So, they must be combined with additional polymers to increase their mechanical integrity.

For a fabricated biomaterial to be bioactive, its composition must have beneficial nutrients for the body during tissue repair. Beginning from the early 2000's, many natural and synthetic polymers were utilized for *in-situ* TE an ideal biomaterial scaffold. The most prominent polymers being collagen, elastin, Polycaprolactone (PCL), Polylactic acid (PLA), Gelatin, Polyether Polyurethane (PU), cellulose, chitosan, and alginate due to their biocompatibility and/or mechanical properties [2–9]. Of natural and synthetic polymers natural are more bioactive, biocompatible, and non-toxic. Synthetic polymers, however, have unique tunable properties [10]. As natural polymers present two (bioactive and biocompatible) of the four desired properties for an ideal biomaterial, they can be more desirable than synthetic polymers.

Over the past 35 years, many techniques have been utilized in order to TE a natural polymer scaffolds. One of the earliest techniques was photolithography. Photolithography, figure 1, works by a light beam (figure 1a) etching into material with a photoresist substrate (figure 1b) underneath the beam. Once the material (silicon in figure 1) is etched onto, the polymer solution is poured into the mold and set [11]. Photolithography has been enhanced from micro- to nanoscale scaffolds structures. It is still used for TE scaffolds but is normally combined with another method or utilized for

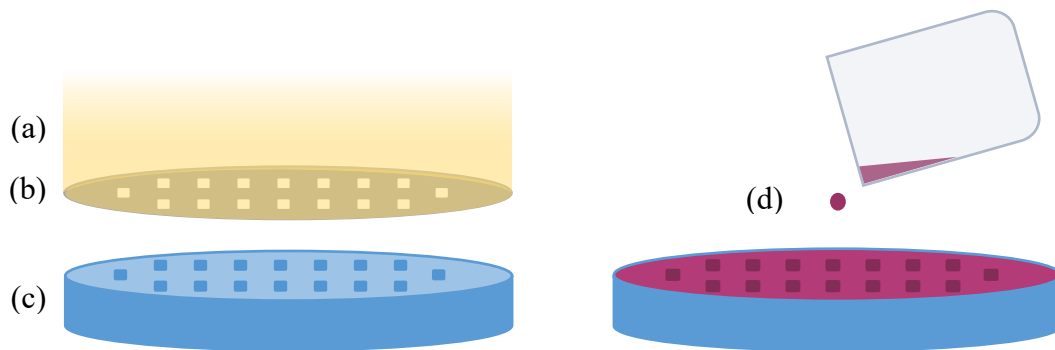


Figure 1: polymer scaffold made through photolithography. (a) is the light source that strikes (b) a photoresist material that only allows selected regions of light to pass through. (c) is the silicon mold that is being etched on. (d) is the polymer solution that will be hardened into a scaffold.

crosslinking scaffolds [12,13]. As time progressed, research showed that the fabrication process of a scaffold strongly controlled the scaffold properties. [14]. Different TE techniques resulted.

As earlier stated, a main polymer used for scaffolds is gelatin. In the 1970's hydrogels which are a combination of water and gelatin were sought after for scaffolds. They did not come into strong use until the 1980's where their bioactive, biocompatible, and biodegradable ability enhanced. However, a hydrogel has a conflicting component of

weak mechanical properties [15] which limited their use initially. Alternative scaffolds became present showing a stronger structure with better mechanical properties. A fabrication technique used in 1990 called Solid Free-form (SFF) was the forway for many fabrication techniques. SFF in combination with computational topology design (CTD), created 3dimensional scaffolds through computer-controlled design. This allowed a strong advantage of pore size of the scaffold to be set. Pore size and fiber dimensions are important for a biomaterial as they can promote or hinder cell growth into the scaffold. An earlier SFF fabrication machine called MSTL created a scaffold by utilizing a UV light to cure liquid polymer in a pattern dictated by the CTD programming. Fused deposition modeling (FDM) followed. FDM works by melting a polymer and extruding it onto a plate in the pattern programmed by the CTD. The pore size for FDM averaged around 350 $\mu$ m but could be as small as 100 $\mu$ m. Both these technique were beneficial for the pore size choice, however, during cell seeding there was inconsistency in cell growth density [16].

A little while later in 1995, 3D printing came to light. Very similar to its predecessor of SFF, 3D printing works by extruding a polymer melt onto a plate determined by a CTD program [17]. 3D Printing has the potential to be scaled-up for industry as it produced scaffolds inexpensive scaffolds at a high rate [2]. However, 3D printing varies fiber diameter of the scaffold based on the extruder diameter. Going past micro into nanofibers has been a challenge. Additionally, the extruder has a limit of viscous polymer solutions that can utilized due to the extruder size [18].

A little after 3D printing in 2004, bio-nanocomposites were starting to be made and similar to 3D printing eventually incorporated into industry. These bio-

nanocomposites are made several ways, essentially with the key components being a polymer absorbing a nanoparticle to polymerize and form a structured scaffold. This can be done with or without a solvent present. Bio-nanocomposites have an advantage of good mechanical strength and low cost [19]. However, a disadvantage of bio-nanocomposites is the degraded particles can be toxic along with poor cell proliferation [16]. A different method that's main focus is to construct nanofibers and pores of a scaffold on a nano-scale is self-assembly. Through self-assembly peptides (the units of proteins) are placed into a salt or physiological solution. The peptides then bond and form together in long chains making nanofibers on the order of 10nm with pores varying from 5 to 200nm [20]. While the size of the nanofibers is beneficially small this can also be a disadvantage. During tissue repair cells need an ideal surface area to pore ratio with which to grow on and proliferate through. Different types of self-assembly focusing on bulk assembly (e.g. molecules, lipids, nanoparticles) are being researched to construct a better surface to pore ratio for the cells to have healthy growth [21,22].

A final TE approach that originated around the 1900's but became popular for fabricating scaffolds in the 2000's is electrospinning. Electrospinning comes in two main forms as direct current (DC) and alternating current (AC) electrospinning. DC electrospinning originated first and has already been implemented into industry. DC electrospinning fabricates a nanofiber by pushing a charged polymer solution through a needle (extruder) towards an oppositely charged collector, figure 2. As the polymer solution is attracted towards the collector the solvent in the solution evaporates producing a nanofiber. This technique can make fiber diameters on the order of 50nm [23]. An

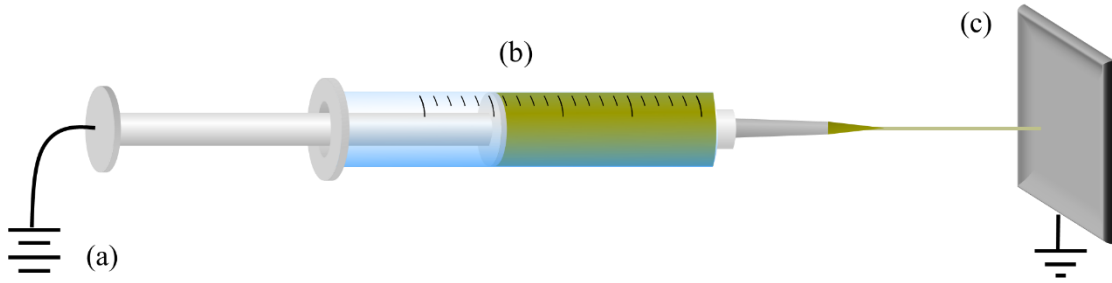


Figure 2: DC electrospinning a nanofiber. (a) is the power supply connected to the (b) syringe which projects a polymer solution forward to the oppositely charged collector (c).

advantage of DC electrospinning is the ability to vary fiber diameter by utilizing more or less polymer in the solution, ultimately affecting porosity. Additionally, electrospinning mimics natural body tissues' fiber morphology [24]. However, a disadvantage to DC electrospinning is the low production rate. Current research has optimized DC electrospinning production rate by applying multiple needles systems. However, the common DC electrospinning machine still has a low production rate and machines with higher production rate are very expensive and limited.

The TE fabrication methods discussed are highlights of many techniques that occurred around the 1900's when TE became popular. From the 1900's to the 2000's, as each biomaterial fabrication method developed and grew so did the knowledge to construction the ideal biomaterial. An ideal biomaterial has four key properties. It is biocompatible in order to mimic natural body tissue in composition and morphology. It must be bioactive to support a physiological environment that cells can proliferate and grow on. Additionally, the ideal biomaterial must be biomechanically viable to sustain any straining or compressing that it would undergo in a patient's body. Lastly, this biomaterial must be mass-producible in order to retain low cost and be fabricated scale-up for industry.

## 1.2 The Backbone of Biomaterial

An ideal biomaterial is a material that can fully mimic the functions and properties of natural body tissue in a physiological environment. This biomaterial needs to have the following four ideal properties: biocompatibility, bioactiveness, biomechanical viability, and mass-producibility. Many years of research has focused on fabricating this ideal scaffold, however, there is still need for further development [25]. Current research in TE has faced a main challenge of poor cell proliferation into fabricated scaffolds. For cell growth to occur, cells need a familiar physiological environment. Leading TE to focus on producing a material that strongly mimicked the natural body tissue morphology [26] and composition.

Natural body tissue's morphology is a base structure called the Extracellular Matrix (ECM), sometimes referred to as a scaffold. The ECM is a random fibrous network (seen in Figure 3) generated as the body's first step of tissue repair. All other

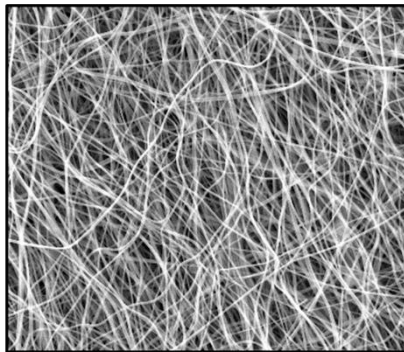


Figure 3: example of an ECM with random fiber morphology.

tissue regeneration components utilize this ECM structure to grow across and heal the injury. The fiber diameters of the ECM range from 50 to 500nm depending on the type of tissue [27]. In addition to morphology, the biocompatibility of the biomaterial is

determined by its composition. The natural body's ECM nanofibers consist of a main polymer called collagen and a fibrous protein, elastin. Fabricating an ECM with a main polymer of collagen or collagen derivative is beneficial to provide a familiar environment for cells to grow on.

This paper presents a material with a random fiber morphology with a base structure of gelatin nanofibers on the order of 200nm in diameter and under. This material has a polymer composition of gelatin (a collagen derivative). Gelatin is a collagen derivative giving it biocompatible properties. Currently, several different types of gelatins are used for TE scaffolds [28]. The most common type of gelatins utilized are from mammalian sources. An alternative to mammalian gelatin is gelatin from fish skin. Fish skin gelatin (FSG) is more ethically kosher than mammalian gelatin. Additionally, FSG is environmentally safer as it is soluble in a pure aqueous solution at room temperature. Avoiding the use of harsh solvents to dissolve the gelatin, further results in ease of use and lowered expense [29–31]. For these reasons, FSG nanofibers are an attractive composition and structure for a biocompatible, bioactive ECM.

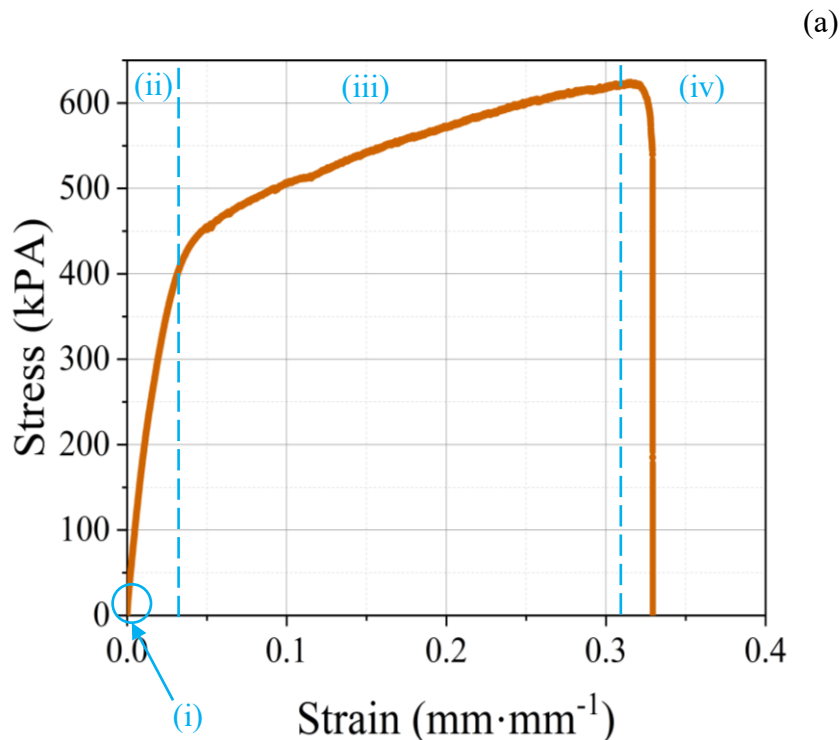
### 1.3 Biomechanical Properties of the Extracellular Matrix

Another property of the ideal biomaterial is biomechanical viability. The proposed main polymer for the ECM composition, gelatin, naturally has poor mechanical properties. In order for a nanofibrous gelatin ECM to be an ideal biomaterial, the gelatin nanofibers need further enhancements to improve their mechanical properties. As FSG is easily soluble in various solutes, FSG solutions can incorporate other polymers for improved mechanical strength. Two polysaccharides that have previously shown to improve gelatin nanofibers mechanical properties are cellulose and chitosan.

Additionally, these polysaccharides are biocompatible with chitosan being antimicrobial giving a further benefit of reducing infection to the patient's injury site [32].

Normal body tissue is a viscoelastic material which is a solid that retains fluid like properties. The solid component of a viscoelastic material is the elasticity of the material which provides shape retention. The fluid like component is the viscosity of the material which is dependent on time. After a viscoelastic material is strained over time the entropy of the material will cause loss of elasticity and the material's viscosity will take over causing dimensional changes in the material.

As such, the most important region for a viscoelastic material is the elastic region [34]. If the material loses its elasticity, then the stretched viscous dominant material will not hold up in a physiological environment. Reducing a viscoelastic material from its time-dependent region of viscosity allows a close focus onto the important elastic region. As natural body tissue is strained the below stress-strain curve, figure 4a, shows a



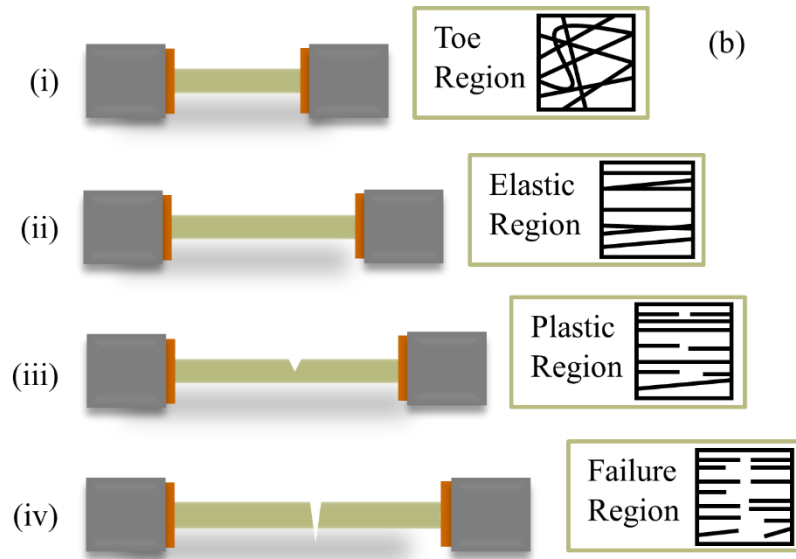


Figure 4: (4a) is stress-strain curve for normal body tissue. (a.i.) is the toe region (a.ii) is the elastic region (a.iii) is the plastic regions (a.iv) is the failure region where the samples breaks. 4b shows the nanofibers orientation as they are being strained.

representation of the materials static region incorporating elasticity, figure 4a.ii. Figure 4b, shows how the natural body ECM's fibers reorientate as they are strained. During initial straining the toe region of the stress-strain curve is created. The fibers have a random morphology that will begin aligning figure 4b.i to 4b.ii as it is strained. This initial stress of the tissue is resulting from the elastin fibers in the ECM. When pulled to the elastic region figure 4a.ii the polymer collagen feels the impact of the stress the most causing a linear region. Once the material is pulled past the elastic region, the fibers in the ECM have failed or have permanent deformation in shape, figure 4b.iii. The material is rendered useless as it cannot longer hold up in the desired physiological environment.

The proposed FSG nanofibers for an ECM mimic natural body tissues' viscoelastic nature [33]. The static stress-strain curve, additionally, allows the elastic

modulus for the material to be determined. This young's modulus will need to be similar to natural body tissue's modulus to provide a bioactive environment for cells to grow. An ideal biomaterial's elastic modulus will vary based on the type of tissue or organ.

For the purposes of this paper, a focused attention was paid to vascular tissue. While literature varies on a desired young modulus due to multiple layered material and other factors, 4-6MPa was chosen as the desired elastic modulus for the gelatin-based material. This is due to the unseeded one-layer nature of the proposed material.

#### 1.4 Mass-producible fabrication

The last property for an ideal biomaterial is scale-up fabrication of the material to implement the biomaterial into industry. While the section *History of Tissue Engineering* proposes many fabrication techniques each technique presents unique benefits and challenges. The needed fabrication technique will vary based on the type of desired tissue. Tissue types vary mainly on composition, soft or hard tissue, and fiber diameter size (50-500nm). As the desired biomaterial is vascular tissue these three previous properties limited the fabrication techniques for small diameter gelatin nanofibers being soft tissue. Additionally, the fabrication technique must be scale-up. As only three of these fabrication techniques mentioned in *History of Tissue Engineering* are implemented into industry, self-assembly, 3D printing, and DC electrospinning, the material fabrication method was further limited for mass-producibility.

Of the three techniques, electrospinning, currently, has an advantage of making soft tissue ECM mimic with controllable thin nanofiber diameters for FSG. This has been successfully done in both previously mentioned DC electrospinning and in its sister technique AC electrospinning [31,35]. In comparison to DC electrospinning AC

electrospinning has several advantages of higher-yield, simpler set-up, and larger range of spinnable polymers. AC electrospinning fabricates nanofibers through a complex electrohydrodynamic process. When an Electric-field is created inside the FSG solution on top of the AC electrospinning machines dielectric disk, figure 5a., the similar charge

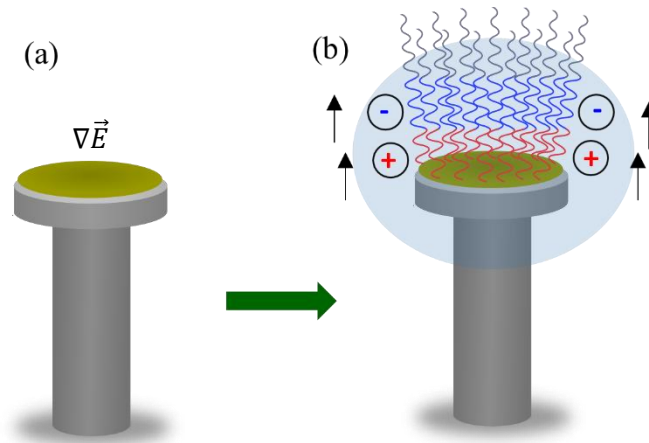


Figure 5: AC electrospinning FSG nanofibers. (a) adapted from *Kennell et al [34]* showing the FSG solution on the electrode before an  $\nabla E$  is created. (b) shows the production of nanofibers after the electrohydrodynamic process starts.

distribution across the surface area of the FSG repels against each other and forces jets of solution to form on the solutions surface. As voltage oscillates the jets relax back into the solution only to be pulsed again when the alternating voltage reaches another peak. This process repeats several times and in less than a second until a layer of nanofibers is formed as seen in figure 5.b. This nanofiber layer has one charge distribution which is the same as previous the surface charge of the solution. On the next voltage peak a layer of oppositely charged fibers is formed below the first layer of nanofibers. The momentum from the bottom fiber layer pushes the top layer away from the disk. While the fibers are

being created (and even the jets) the high voltage is also charging electrons in the air that are flowing away from the electrode. This flow of electrons or electric wind lifts the nanofibers away from the electrode towards a collector. Once these charged nanofibers reach a specific distance from the plasma ball of air created around the electrode, the charged fibers relax to a more comfortable state of neutrality through charge recombination inside of the nanofiber. The uncharged nanofibers then reach the collector to form the nanofiber material.

After easy removal of the nanofibrous material from the collector, the material has an ECM morphology. Electrospinning has a natural affinity to mimic the body's ECM. AC Electrospinning is capable of starting the first step in tissue healing with creation of the ECM [35]. Additionally, electrospinning can produce controlled fiber diameters on the order of 100 to 1100nm which allows a large range for specific fiber diameters in the ECM [18]. Fiber diameter control is beneficial for fabricating a specific desired tissue.

In addition to control of the materials morphology, electrospinning can spin a solution with main solute of water. FSG in a pure aqueous solution was spun at a flow rate of 0.5mL/h in DC [31] and 36mL/h in AC [34]. AC electrospinning has a higher production rate of gelatin nanofibers by four times than any other material fabrication technique [35]. Due to AC electrospinning high-yield, control of nanofiber diameter, ability to mimic the body's ECM, and ease of use, it is an ideal fabrication method for the proposed biomaterial platform.

## 1.5 Hypothesis and Aims

Creating an ideal biomaterial that is biocompatible, bioactive, biomechanically viable, and mass-producible would have strong impacts in the field of medicine. This

biomaterial would be beneficial during transplant surgeries as it would dispense the need for an organ donor or second surgical procedure on the patient to obtain tissue.

The hypotheses proposed by this research is can an AC electrospin nanofibrous fish skin gelatin extracellular matrix be utilized as a platform for tissue repair. This FSG ECM would need to retain the four main important properties of a biomaterial which are the following: biocompatibility, to avoid an immunogenic response, bioactivity, to provide cells with a healthy physiological environment, biomechanically viable, to provide good mechanical sustainability preventing tissue failure, and mass-productibility, to allow industrial level production. After initial proof of concept, alternating current electric spinning can fabricate an innovate fish skin gelatin nanofibrous extracellular matrix which will be tested for the four main biomaterial properties.

The first aim, of this research is to validate that AC Electrospinning can be used to fabricate a FSG nanofibrous ECM scale-up for industry. As well as verifying the bioactive and biocompatibility nature of this FSG ECM. This aim presents a FSG nanofibrous material with a similar morphology and composition to natural vascular tissue with favorable cell growth at a high production rate.

The second aim of this research will be to enhance the mechanical properties of the FSG material, in order to create an ideal biomaterial that is biomechanically viable. Combined with biomechanical viability, this FSG nanofibrous ECM needs to degrade slowly in physiological environment to allow the body's vascular tissue to selfheal. Further insight into the effect of the ECM biodegradability on the mechanical properties of the material will be paid attention to. This aim presents a biomechanically viable FSG ECM with similar biomechanically properties to vascular tissue, and enhancement of the

mechanical properties through additional polymers and post-processing treatments to slow the degradation rate giving a more mechanically sound biomaterial.

FISH SKIN GELATIN NANOFIBROUS SCAFFOLDS SPUN USING  
ALTERNATING FIELD ELECTROSPINNING AND *IN-VITRO*  
TESTED WITH TDTOMATO MICE FIBROBLASTS

by

AMANDA KENNELL, MARK MACEWEN, MICAH ARMSTRONG, TEODORA  
NICOLA, BRIAN HALLORAN, NAMASIVAYAM AMBALAVANAN, ANDREI  
STANISHEVSKY

Submitted to *Materials Communication Today*

Format adapted for dissertation

**Fish skin gelatin nanofibrous scaffolds spun using alternating field electrospinning and *in-vitro* tested with tdTomato mice fibroblasts.**

Amanda Kennell<sup>a\*</sup>, Mark MacEwen<sup>b</sup>, Micah Armstrong<sup>c</sup>, Teodora Nicola<sup>b</sup>, Brian Halloran<sup>b</sup>, Namasivayam Ambalavanan<sup>b</sup>, Andrei Stanishevsky<sup>a</sup>

<sup>a</sup> *Department of Physics, University of Alabama at Birmingham, Birmingham, AL 35294, USA*

<sup>b</sup> *Department of Pediatrics, University of Alabama at Birmingham, Birmingham, AL 35249*

<sup>c</sup> *Department of Materials Science and Engineering, University of Alabama in Birmingham, Birmingham, AL 35233*

\*corresponding author email: [akennell@uab.edu](mailto:akennell@uab.edu), postal address: University of Alabama at Birmingham, 1300 University Boulevard, Birmingham, AL 35294-1170, USA

## **Abstract**

There is a strong need for the mass production of biomaterials, as tissue engineering shows promising results in transplant surgeries. This research presents preliminary results on a “green” method of constructing a biomaterial that is bioactive, biocompatible, and suitable for scale-up manufacturing. This was done by producing nanofibrous fish skin gelatin (FSG) scaffolds from an aqueous precursor using a high throughput alternating field electrospinning (AFES) method. The nanofibrous FSG material was produced at 12.6 g/h and could include carboxymethyl cellulose (cmCEL) as an additive to improve mechanical properties. To keep the process environmentally safer, thermal crosslinking was used to control the scaffolds biodegradation rate and maintain a uniform fiber diameter distribution of  $175\pm 19$  nm. Scanning electron microscopy indicated similarities between the scaffold and the extracellular matrix (ECM). The scaffold’s biocompatibility was verified with *in-vitro* testing utilizing naturally fluorescent tdTomato mice fibroblasts. The cmCEL loaded FSG scaffold demonstrated 11.5% higher cell proliferation after 72 h compared to the pure FSG scaffold. Also, the cmCEL loaded scaffolds had more uniform cell distribution ( $235\pm 80$  cells/mm<sup>2</sup>) than the FSG scaffold ( $251\pm 179$  cells/mm<sup>2</sup>). The results demonstrate a uniform nanofibrous ECM with favorable cell response can be reproducibly made with a high productivity rate through AFES.

**Key Words:** Alternating Field Electrospinning, Nanofibers, Fish Skin Gelatin, tdTomato Mice Fibroblasts, Extracellular matrix

## 1. Introduction

Tissue engineering (TE) with nanofibrous materials shows promising results in transplant surgeries where there is a strong need for a sustainable production of natural biomaterials. Tissue repair starts by making an extracellular matrix (ECM). Developing a structure that mimics the ECM (ECM mimic) has had a limited rate of success [1]. Also, the issues for safely developing this backbone, the ECM mimic, have not yet been overcome. Electrospun natural biopolymers are attractive for developing this ECM mimic but their production is very limited. This study proposes a “green” electrospinning method to overcome some current limitations in TE to make a viable, sustainably, and manufacturable ECM mimic.

The body’s natural response to heal from a trauma is laying a collagen web called the ECM. This ECM web consists mainly of collagen with elastin, fibrin, and other macromolecules [2]. In order to skip this first step in tissue repair, an ECM mimic can be made from an electrospun nanofibrous scaffold. As collagen makes up the largest portion (30%) of the ECM [2,3] many current scaffolds are made from collagen [4]. However, electrospinning a collagen scaffold is difficult, as collagen needs harsh chemicals to become soluble. Additionally, collagen has been suspected to transfer diseases to its host through prions [5,6]. Collagen also needs additives such as fibronectin to further promote cell proliferation and control the ECM’s degradation rate [7]. Another necessary additive is elastin (also natural to the body’s ECM) which makes the collagen based ECM malleable enough [8]. Fibronectin and elastin are expensive and time consuming to process and electrospin, which further complicates the collagen ECM’s process.

Ideal biomaterials must demonstrate an optimal level of biocompatibility, biodegradability, and bioactivity to induce a favorable response from the body's immune system. Even though collagen is natural it has deficiencies, as mentioned previously, in electrospun productivity rate and unfavorable use of harsh solvents. Gelatin, a derivative of collagen, has more desirable properties [9,10] for an ECM mimic. Gelatin is easier to electrospin than collagen, it has been shown to not transfer diseases to its host [6], and it is more environmentally friendly as it can be fully soluble in a pure aqueous solution [11]. On its own gelatin is naturally elastic [10] indicating that there is no need for additives to improve a gelatin ECM's elasticity. Gelatin also stimulates cell proliferation [11,12], is biodegradable [11], and has a controllable biodegradation rate through crosslinking. However, the mechanical properties of gelatin alone are not fully suitable for an ECM [13]. Electrospinning of gelatin nanofibers is very versatile so additives (such as polysaccharides) can be easily incorporated with gelatin to overcome the mechanical inadequacies [14]. Overall, gelatin presents itself as a promising main polymer for an ECM mimic.

Gelatin comes mainly from two main sources: porcine and calf skin. Recently, an increased attention has been paid to gelatin from fish skin (FSG) [5,6]. Utilizing FSG has several benefits to calf skin gelatin as several studies have placed warning that Bovine Spongiform Encephalopathy (BSE) might be transmittable to the host from calf based gelatin [11,12,15]. In addition, FSG is more ethically kosher [5,6] meaning a larger population will be willing to have a transplant surgery with an FSG ECM mimic. Alternatively to calf skin and porcine, FSG can be dissolved in and electrospun from a pure aqueous solution [11]. These qualities make FSG attractive for lowering costs,

disbanding with harsh solvents, simplifying syntheses of complex materials, and more creating ethically kosher materials.

Previous studies have demonstrated the syntheses of sustainable ECMs made from gelatin nanofibers and films [16]. This was done by targeting the tissue's ECM morphological properties. The main ECM properties are a random fiber morphology with fiber diameters ranging from 50 to 500 nm [17], a porous structure to allow cell migration [18], and a controlled degradation rate to prevent cells from degrading with the ECM [10]. All these factors point to utilizing electrospun and crosslinked gelatin nanofibrous materials. An advantage of the electrospun method is its natural ability to make a nanofibrous ECM mimic from nanofibers [16]. Further, the degradation rate can be controlled through different methods of crosslinking, e.g., thermal crosslinking, ensuring they are environmentally safe [13].

Some current methods utilized to make gelatin nanofibers can produce the fiber diameter, scaffold porosity, and morphology requirements with a con of a non-aqueous solvent. However, a “green” method suitable for scale-up production has not been fully achieved. One of the current methods used for gelatin nanofiber construction is centrifugal spinning (C-Spin). C-Spin's main attraction is its simplistic set up to produce fibers [19]. However, ECMs produced by C-Spin have shown poor cell migration into the scaffold [20]. This is due to a large range of fiber diameters on the micro to nanoscales, as two papers indicated gelatin nanofiber diameters ranging from 265 to 632 nm [19–21] which is within the necessary diameter range for the ECM, but are non-uniform [17] further resulting in a low porous scaffold [20]. This method is usually combined with another method (i.e. electrospinning) to overcome these barriers [19,22] taking away from the simplistic set up. As C-Spin usually needs another method

to create a good ECM mimic and there are no published flow rates for C-spinning, utilizing alternative synthesis methods for gelatin ECMs is desirable.

Another current method to construct gelatin nanofibers is solution blow spinning (SBS) also referred to as airbrushing [23]. The benefits of SBS is its inexpensive set up and the ability to make versatile fiber compositions [24]. Gelatin fibers have been spun at a flow rate of up to ~1.2 g/h (while others have reported a rate of 1.2 to 2 g/h with SBS) [25,26]. The fiber diameters were as small as 67.5–98.3 nm meeting the tissue's ECM fiber diameter requirement. As seen by the fiber diameter size and good pore size, SBS ECM mimic allows good cell proliferation [23]. Even with this strong benefit of SBS, utilizing another method with a higher production rate would be beneficial for industrial level production.

An alternative method for gelatin fiber construction is Direct Current (DC) electrospinning. Gelatin nanofiber diameters as small as 48 nm have been made with DC electrospinning [27]. The fiber diameter produced by DC electrospinning is uniform providing a suitable surface area to pore size ratio allowing cells to proliferate across the ECM mimic [28,29]. DC electrospinning has a natural ability to construct an ECM mimic [13]. However, a single capillary DC flow rate is slow averaging at 35–81.6 mg/h [27,30,31]. A milestone of “green” electrospinning was when DC electrospinning spun fish gelatin fibers for the first time from a purely aqueous solution [11]. Even though DC electrospinning can make suitable nanofiber compositions these fibers are electrically charged and must be neutralized before removal causing user risk. While DC electrospinning meets many of the tissue's ECM requirements, this method's production rate is slow and an requires additional neutralization step.

Each of the described methods present benefits and drawbacks from making the ideal ECM. This paper presents a newer method called alternating field electrospinning (AFES) to combine the benefits of the above spinning techniques to construct a better ECM for scale-up production. In this present work, FSG NF's diameters ( $\leq 300$  nm) were successfully prepared at six times higher the rate compared with the current methods. AFES is a high-yield electrospinning technique that has the same advantages as DC electrospinning which are: large surface area to pore size ratio, small nanofiber diameter, and easily varied fiber composition with the additional benefits dense nanofiber flow with no electric charge, high production rate, scale-up production, easy fiber collection, and NF collection without a grounded collector [32–34]. This makes AFES a less expensive and more flexible method to construct a FSG nanofibrous ECM mimic. The ability of AFES to electrospinning porcine and calf skin gelatin has been demonstrated, however, no properties of the scaffolds were tested [35]. Therefore, utilizing AFES to electrospin FSG for an ECM would combine the benefits of both the method and polymer as a viable ECM mimic.

The goal of this study was to develop a “green” AFES method to fabricate a FSG ECM mimic for scale-up production. To keep this method environmentally friendly, in addition to the AFES spinning of FSG NFs from a purely aqueous solution, the nanofibers were crosslinked with no chemicals. AFES was successfully applied at a production rate of 12.6 g/h making FSG nanofibers with an average narrow and uniform, crosslinked NF diameter range of 100–200 nm. Characterization of cellular response to the fabricated ECM was *in-vitro* tested using naturally fluorescent tdTomato mice fibroblasts that allowed live imaging. These naturally fluorescing cells eliminated an extra dying step and avoided subjecting the scaffold to chemicals that can cause

morphology changes in the scaffold making cells pop out of the ECM. This study's results on "green" FSG ECM mimic made by using AFES are presented below.

## **2. MATERIALS AND METHODS**

### **2.1. Precursor Preparation:**

The initial precursors of the biomaterial were made using gelatin from cold water fish skin (Sigma-Aldrich, viscosity 7.0-10.0 CS and pH 4.0–7.5 in 10 wt% solution at 30 °C). Four different FSG precursors were made with 31 wt% FSG in 85–100 wt% of deionized water (dH<sub>2</sub>O) solvent with the remainder being acetic acid (AA) (Alfa Aesar, glacial, 99+%). The precursors were then stirred with a Thermix Stirrer (Fisher Scientific, Model 220T) at room temperature. Three more precursors were made with (0, 0.5, 1 wt%) Carboxymethyl cellulose sodium salt (cmCEL) (Scientific Polymer Products, viscosity 1–20 cp at 2 wt% H<sub>2</sub>O) with 85–100 wt% dH<sub>2</sub>O solvent and the remainder being AA. The more cmCEL contained in the precursor the higher the amount of AA that was required for the cmCEL to be fully dissolved. After fully mixing, FSG 31 wt% was added and stirred with the Thermix Stirrer at room temperature until fully dissolved. All the precursors were AFES spinnable for a period of at least one month after preparation.

### **2.2. Electrospun Nanofibrous Scaffolds**

In a typical process of AFES 30 ml of precursor, Figure 1a, is placed into an automated syringe pump that delivers the precursor to a flat electrode with a 25 mm diameter, Figure 1biii-iv. An AC voltage of 26–39 kV rms voltage is applied to the electrode causing nanofibers to be produced up to 12.6 g/h. The nanofiber flow was driven by electric wind phenomena as a cylindrical mesh shape indicating continuity of

long nanofibers, Fig 1bii The nanofibers are collected on a rotating plastic cylinder with a diameter of 10cm, Fig 1bi Nanofibers were produced until a nanofibrous layer thickness reached approximately 200  $\mu\text{m}$  taking 15–30 min depending on the precursor. The nanofiber layer was easily removed from the collector to form a sheet, Fig 1c These nanofibrous sheets (20 $\times$ 25 cm) were then dried in a vacuum chamber for 24 h at room temperature.

### **2.3. Crosslinking and UV Sterilization**

The dried NF sheets were next crosslinked to prevent dissolution in an aqueous solution. The chosen crosslinking method was thermal crosslinking with a temperature ranged from 160  $^{\circ}\text{C}$  to 180  $^{\circ}\text{C}$  in an Isotemp Programmable Muffle Furnace from Fisher Scientific. To choose the prime crosslinking time and temperature, a degradation experiment was performed on the sample FSG, FSGAA-5, and FSG/CEL-5. The nanofiber sheets were crosslinked at two different temperatures and time periods to find this optimal crosslinking procedure: 160 $^{\circ}\text{C}$  for four hours, 160 $^{\circ}\text{C}$  for eight hours, and 180 $^{\circ}\text{C}$  for four hours. For each temperature three samples of FSG, FSGAA-5, and FSG/CEL-5 were used. After crosslinking, the mass and density of each sample were determined. The samples were then immersed in Dulbecco's phosphate buffer saline solution with Ca and Mg (DPBS) (Mediatech) for two time periods, one day and 7 days, in a CO<sub>2</sub> incubator (Lab-Line) at 37 $^{\circ}\text{C}$  (normal body temperature). The samples were rinsed in dH<sub>2</sub>O and left to fully dry at room temperature. Once dried, the samples were reweighed to determine the mass retention.

After finding the optimized crosslinking time and temperature based on which samples had the most mass retention, the samples from Table 1 and 2 were crosslinked at the optimized thermal crosslinking procedure of 160 $^{\circ}\text{C}$  for eight hours in an Isotemp

Programmable Muffle Furnace 650 (Fisher Scientific). Afterward, the NF sheets were cut into discs and placed in a 24 well plate. The samples were briefly exposed to UV light for 10 minutes for sterilization. To determine the effects of thermal and UV treatment, infrared spectroscopy (IR) was performed on these nanofibrous matrices after each stage (before crosslinking, after crosslinking, and after UV sterilization) by using a Fourier Transform Infrared (FTIR) Vertex 70 FTIR spectrometer (Bruker Optics) in transmission mode at a resolution of  $2\text{ cm}^{-1}$  and an average of 32 scans per sample.

### **2.5. SEM Analysis of Nanofibers**

The nanofiber samples were imaged after each of the three stages of fabrication using the scanning electron microscopy (SEM, field-emission scanning electron microscope FEI Quanta 650 FE-SEM), to observe the changes in the matrix's microarchitecture and fibers' morphology. Before SEM imaging, the samples were sputter-coated with a layer of AuPd. After sputter coating to reduce the samples electric charge, the samples were placed in the SEM chamber with a base pressure of  $1 \times 10^{-4}$  Pa. SEM images were taken in secondary electron mode with an accelerating voltage of 15 kV, the electron probe current set at  $2.5\ \mu\text{A}$ . ImageJ image processing software was then used on the SEM images to determine the nanofiber diameters in each sample before and after crosslinking. A histogram of the nanofiber diameters distribution was constructed for each set of samples.

### **2.6. Tensile Testing**

Preliminary analysis of elastic properties of nanofibrous FSG sheets were carried out using ADMET eXpert 4000 micro tester. The device was equipped with a 5N load

cell, MTESTQuattro controller and software. The samples were placed in the custom-made bath and fixed using microclamps with the gauge length set as 10 mm to achieve up to 250 % strain. The sample widths were between 2 and 5 mm. All tests were performed in the custom-made bath in SBF at 37 °C and repeated at least 3 times for each material.

## **2.7. *In-Vitro* Testing**

*In-vitro* testing was performed on the FSG scaffolds with tdTomato Mice Fibroblasts. Cell media (containing 40,000 cells) was pipetted onto each sample in the well plate. Then the samples (thickness of 200  $\mu\text{m}$ ) were placed in an incubator and kept at 37°C. They were checked for cell growth after 24 h, but no noted cell growth was observed on the FSG ECM (a few cells per  $\text{mm}^2$ ). There was still relatively little cell growth observed after the 48 h time period. However, after 72 h the cell growth significantly expanded, and the scaffolds were imaged with a microscope (Nikon Eclipse TE-2000U). A few samples were lost during aspiration. Afterwards, Invitrogen-ProLong Diamond Antifade Mountant with DAPI (Thermo Scientific Fisher) was used to stain the tdTomato mice fibroblast's nuclei (as the rest of the cell naturally pre-fluoresces) and fix the cells. The samples were then mounted onto microscope slides.

The mounted samples' cell growth was viewed with a microscope (Nikon Eclipse TE-2000U), Figure 7. The program Nikon was used to take fluorescent images of the cell growth. Each sample had two images taken of the front and back of the sample. Afterwards, the software ImageJ was used to determine the confluence of the cells, Figure 8a-b. The region statistics of the sample's two pictures were averaged to obtain a uniform distribution on each sample. ImageJ was again used to identify the number

of cells/mm<sup>2</sup> on the samples. The two pictures of each sample were again averaged together for a uniform number of cell nuclei on each sample, Fig 8a.

## **2.8. Fluorescing Live Cells**

*In-vitro* testing was again performed on the FSG scaffolds (thickness of 400 μm) with tdTomato Mice Fibroblasts. Cell media (containing 200,000 cells) was pipetted onto each sample in the well plate. More cells and thicker scaffolds were used to gain a more uniform cell proliferation on scaffolds. Then the samples were placed in an incubator and kept at 37°C. After 72 h, cell growth was observed with a microscope (Nikon Eclipse TE-2000U). The scaffolds were removed from the incubator after 72 h of cell growth, and placed in new cell media. Two drops of NucBlue (ThermoFisher Scientific) was added to each well per milliliter of cell media. After 20 min of incubation at room temperature, these scaffolds were imaged live with the Nikon Eclipse TE-2000U microscope.

## **2.9. Fixing cells**

*In-vitro* testing was performed on the FSG scaffolds (thickness of 200 μm) with tdTomato Mice Fibroblasts. Cell media (containing 190,000 cells) was pipetted onto each sample in the well plate. Higher cell plating was done to ensure large cell growth after 48 h. Then the samples were placed in an incubator and kept at 37 °C. After 48 h, cell growth was observed with a microscope (Nikon Eclipse TE-2000U). The samples then underwent cytoskeleton staining. The scaffolds were rinsed in PBS to remove the cell media. Next, they were fixed with 3.7% methanol-free formaldehyde. The scaffolds were rinsed again with PBS and then permeabilized with 0.1% Triton X-100 in PBS. The scaffolds were again rinsed in PBS. To stain the cell's cytoskeleton two drops of ActinGreen<sup>tm</sup> 488 Ready Probes® Reagent was added to the cell's media per milliliter

of media. After 30 min of incubation at room temperature the ActinGreen solution was removed, and the scaffolds rinsed in PBS again. The scaffolds were then mounted on slides and imaged with the Nikon Eclipse TE-2000U microscope. ImageJ was then used to determine the cell area for each scaffold.

### **3. Results and Discussion**

#### **3.1. Precursor electrospinning and nanofiber production rate**

AFES was easily used to electrospin the aqueous precursors listed in Table 1 at a high production rate up to 12.6 g/h. The fully aqueous FSG precursor had the highest flow rate of 36 mL/h. The production rate of AFES was 200 times higher than that reported for DC electrospinning [11]. There was no difference in the flow behavior or nanofiber diameter when changing the electrode size (from 6 to 37.5 mm diameter) or using more than one electrode to increase the productivity. All the precursors in Table 1 exhibited a healthy flow of nanofibers seen in Figure 1b. These nanofibrous flows have a continuous funnel shape while being electrospun. This continuous shape is indicative of long continuous nanofibers. These nanofibers collected onto the cylinder (100–200 rpm, Figure 1bi.) were easily removed from the collector as the final product of AFES nanofibers are uncharged. This is due to the virtual counter electrode created during AFES [36]. The final weight of the FSG nanofiber sheet was 12.6 g after one hour of spinning. This high production rate, ease of machine use, and versatile solution spinning showed that AFES was a good technique to make gelatin nanofibers.

#### **3.2. Thermal Crosslinking**

As FSG NFs are completely soluble in an aqueous solution controlling their degradation rate is important for their insertion into a biological environment.

Crosslinking has been shown to control nanofibers dissolution rate in an aqueous environment [37]. Thermal crosslinking was chosen because it is environmentally friendly and cost efficient. The only byproduct of thermal crosslinking gelatin NFs is H<sub>2</sub>O [38] and no other costly chemicals are needed to crosslink these fibers. As the only byproduct was water, the nanofibers, Figure 1d-e., showed no visible discoloration or stretching/ tearing after removal from the furnace. This indicated no macro-scale morphological changes due to thermal crosslinking. On a micro-scale, seen in the SEM images in Figure 2a-b., the porosity of the FSG nanofiber sheets decreases as the pores with predominantly triangular shapes shrink a little. This has advantages and disadvantages. A cell needs a certain pore size to proliferate through. If the pore size is too small the cell will not proliferate, and if the pore size is too large the cell will be unable to stay in the ECM due to a bad surface to pore ratio. Finding the optimal crosslinking type and time exposure was necessary for these FSG nanofibers to have this optimal pore size to surface area ratio.

### **3.3. Nanofiber Diameter**

Uniformity of the nanofibers in the nanofibrous sheets is important to provide the cells with consistent nutrients to ingest the nanofibers and proliferate across the sheets. To verify the uniformity of the nanofiber sheet, the non-crosslinked nanofiber diameter measurements were plotted as a histogram, Figure 2a. and then the thermally crosslinked nanofibers at 160° for 8 hours were plotted as a histogram, Figure 2b. The thermally crosslinked nanofiber means with their standard deviations were FSGAA-10 at 175±31 nm, 1 FSGAA-5 at 150±21 nm, FSG/CEL-5 at 175±19 nm, and FSG at 175±41 nm. These nanofibers showed an increase in uniform distribution after thermally crosslinking. This can be seen by the histogram peak being skewed towards

the middle. Additionally, all of the nanofiber diameters meet the requirements of the tissues' ECM fiber diameter range of 50–500 nm [17]. The fiber averages were then compared before and after crosslinking seen in Fig 2b. This graph indicates a decrease in fiber diameter after crosslinking for FSG, FSGAA-5, and FSG/CEL-5. This is because the main non-harmful byproduct of thermal crosslinking, H<sub>2</sub>O, is being removed causing the nanofibers to shrink in diameter [38]. However, the FSGAA-10 showed an increase in fiber diameter when crosslinked. These fibers still showed a loss of H<sub>2</sub>O, however, their fiber diameter increase indicated a lateral shrinkage rather than axial. A statistical test, an Anova, was run on the crosslinked nanofiber diameters showing the crosslinked compared to non-crosslinked nanofiber diameters were statistically different. Overall, AFES naturally produces small uniform fiber diameters for the polymer FSG, and thermal crosslinking caused a relatively small axial and lateral fiber shrinkage giving a better fiber uniformity. This provides an even thinner ECM which is necessary for some of the bodies tissue.

### **3.4. Density of Nanofiber Sheets**

To further validate the uniformity of the nanofibrous (NF) sheets, mass density tests were performed to ensure that the nutrients were distributed evenly across each section of the NF sheet. The nanofiber sheets' FSG, FSGAA-10, FSGAA-5, and FSG/CEL-5 density was plotted as a histogram, Figure 4, for each of the thermal crosslinking temperatures and procedures. These histograms show a normal distribution with the mean of FSGAA-10 at 0.04 mg/cm<sup>3</sup>, FSG/CEL-5 at 0.02 mg/cm<sup>3</sup>, FSG at 0.06 mg/cm<sup>3</sup>, and FSGAA-5 at 0.025 mg/cm<sup>3</sup>. The SD varied between 10–20 % for each NF sheet sample. Even across the varying thermal crosslinking procedures the nanofibers' density stayed uniform. To verify if the uniformity of the produced material, several NF

sheets with 30x150 cm were produced in a test scale-up process. No statistically significant variations in fiber diameter, NF sheet mass density, and pore shapes or sizes were noted for either small or large NF sheets prepared from the same precursors and at same AFES parameters. All the density histogram distributions stayed relatively within the SD of each other's different crosslinking procedures. The only exception was the pure FSG NF sheet crosslinked at 160 °C for 8 h. The density of the sample within itself was uniform, however, the sheet had a much higher density of mean 0.06 mg/cm<sup>3</sup> than the other pure FSG nanofiber sheets crosslinked with varying procedures. A t-test was run to show that the FSG NF sheet crosslinked at 160 °C for 8 h had a statistically significant difference compared to the other two FSG NF sheets crosslinking time and temperatures, Figure 4. This was due to the larger volume shrinkage in this FSG nanofiber sheet. Due to non-Newtonian nature of FSG viscosity [39,40] at this temperature and time a density increase is caused. Overall, the thermal crosslinking procedure can vary the fiber's density, but not uniformity within itself. The small amounts of additives also did not affect the nanofiber sheet's density uniformity. As such, the uniformity of the nanofiber's density is independent of the AFES parameter or the size of the produced NF sheet, crosslinking time and temperature and small variations in nanofiber composition, but dependent on the main polymer and solvent.

### **3.5. Confirming the ECM Structure**

As mentioned previously, cells need a good surface area to pore ratio to grow and proliferate across [41]. This desired surface area structure is seen as the normal tissues' ECM structure [28,42]. All AFES spun NF sheets were imaged using SEM to confirm this random fiber morphology structure of the ECM. The ECM structure of the nanofiber sheets can be seen in Figure 1 or Figures 2. Just as the process of DC

electrospinning nanofibers mimics the ECM structure [10,13] so does AFES NF mimic the ECM structure of the natural body. Even after thermal crosslinking the nanofiber sheets the ECM structure remains with a small decrease in pore sizes Fig 2a compared to Fig 2b. When cells are seeded to this nanofibrous ECM structure they still have a good pore size to surface area ratio to attach to and proliferate across with these novel environmentally friendly FSG NF ECMs constructed at a high production rate.

### **3.6. Degradation tests**

Once the nanofibrous ECM structures are inserted into a biological environment controlling the degradation rate of these structures is vital for proper cellular reproduction. If the ECM degrades too quickly the cells will degrade with the ECM as they haven't been able to establish full growth [10]. If the ECM does not degrade quickly enough this could cause an immunogenic response of the body to attack the ECM. As such the FSG ECM NF sheets underwent degradation tests at the three varying crosslinking times and temperatures. The percentage of mass retained of each of these ECM can be seen in Figure 5. The FSG nanofiber ECM that were thermally crosslinked at 160 °C for 8 h retained the most mass over the 2-week period. As such all nanofibrous ECMs were crosslinked at 160 °C for 8 h for *in-vitro* tests. The other crosslinking procedures would have caused the cells to degrade and be lost with the ECM. Also seen in Figure 5a-5c the addition of cmCEL to the FSG ECM strengthened its integrity further slowing its degradation rate. These degradation tests indicated thermal crosslinking can be used as a "green" method to control fibers degradation rate while the importance cmCEL additives can further slow the degradation rate of the nanofibers.

### **3.7. Mechanical Behavior of FSG Scaffolds in SBF**

The tensile behavior of all scaffolds immersed in SBF at 37 °C demonstrated

similar behavior after either 1 day or 3 days exposure. The recorded engineering stress-strain curves exhibited an extended toe region (from 50 to 150 % strain) due to the gradual realignment of nanofibers along the direction of stretching followed by a linear segment. The linear segments were used to determine the Young's moduli (Table 3) that has been shown to affect the cells viability, *proliferation*, and spreading. The elongation at break was more than 200 % for all samples, which hindered the determination and comparison of maximum stress due to the limit of the instrument. The Young's moduli of the samples exposed in SBF for 24 h increased in the sequence FSG < FSGAA-5 < FSGAA-10 < FSG-CEL-5. The numbers varied, respectively, from ~5.6 kPa for FSG to 32.8 kPa for FSG-CEL-5, with other materials being between. Most scaffolds still maintained 69–85 % of their maximum moduli after 72 h in SBF, except FSG sample (10–16 %) that degraded faster.

The increase of strength and elastic modulus of polymer nanofibers with the addition of cmCEL has been observed [43, 44]. When compared to the scaffold mass density in Fig.4, it can be noted that FSG-CEL-5 and FSGAA-5 scaffolds have the lowest density. Because the both tensile strength and modulus depend strongly on the density of porous material [45], this means that the individual fibers in FGAA-5 may actually have higher modulus than those in FSGAA-10 scaffold. Those factors can explain a better cell initial attachment and proliferation on FSG-CEL-5 and FSGAA-5 scaffolds. The elastic moduli of the scaffolds are slightly lower than those for the human body ECMs but still give the cells a suitable substrate to grow on.

### **3.8. FTIR on Nanofiber ECMs**

To further validate the uniformity and degradation of the nanofibrous ECMs FTIR was used to confirm any molecular structural changes in the nanofibers. The FITR

graphs before thermal crosslinking, Figure 6b indicate no strong differences in the absorption bands other than the cellulose band seen at  $1000\text{ cm}^{-1}$ . The molecular structures after thermal crosslinking the scaffolds at  $160\text{ }^{\circ}\text{C}$  for 8 h also show no molecular structural changes compared to the non-crosslinked fibers. However, after sterilizing these scaffolds with UV light (which slightly crosslinks) minimal oxidation of the FSG/CEL-5 nanofiber ECM can be seen in the band region  $1700\text{ cm}^{-1}$  Figure 6a. While thermally crosslinking causes no degradation, UV sterilization can cause some molecular degradation. This is not enough degradation to affect the cell growth but utilizing a different sterilization method could improve cell growth by preventing the loss of the cellulose additive. These FTIR graphs show again that using thermal crosslinking compared to other kinds of crosslinking retains the uniformity and molecular structure of the original nanofiber composition.

### **3.9. Analyzing Cell Growth**

The uniform nanofiber scaffolds were confirmed to be a biomaterial with a successful *in-vitro* testing of tdTomato fibroblasts. Figures 7a-d shows that the FSGAA-5 scaffold had the largest confluence of cells across it at 14.4%. The main differences in this scaffold were a smaller fiber diameter and a lower density. These two factors provided a better surface area to pore size ratio for the cells to spread across. The pure FSG ECM had the largest number of cells per area ( $251\pm 179\text{ cells/mm}^2$ ) and also the largest density per unit area providing a large surface area for cells to seed into, however confluence was lower due to smaller pore size of the denser material. The FSG/CEL-5 ECM had the largest amount of confluence 11.4% with the least cells  $198\pm 104\text{ cells/mm}^2$ , giving this ECM the largest cells. The only variation between the FSG/CEL-5 ECM and FSGAA-5 ECM was the addition of the cellulose. The effect of the cellulose

additive in the ECM was very beneficial as it provided more nutrients to the cells that attached allowing them to grow larger and stabilize. This is seen when comparing the FSG/CEL-1 and FSGAA-15 ECMs, Figures 8c and 8f. The only difference was the 1 % cmCEL which increased confluence by 9 % overcoming any side effects caused by the AA with a cell number of  $235 \pm 80$  cells/mm<sup>2</sup>. Overall, these ECMs showed good, healthy cell growth and proliferation. The factor that affected the cell growth the most between the AFES spun nanofiber sheets density, nanofiber diameter, ECM structure, surface to area ratio (pores size), the composition (molecular structure), and pore sites. The composition of the nanofiber was the strongest factor of affecting cell growth as seen between the FSGAA-15 and FSG/CEL-1 ECMs. Additionally, increased amounts of cmCEL decreased the SD of the cell number in the ECM causing more uniformity. However, increasing the surface area to pore size ratio of these FSG/CEL nanofiber dimeters (to the FSG fibers density) might further provide more sits for cells to attach and proliferate across the ECM.

### **3.10. GFP fluorescing compared to tdTomato**

The tdTomato mice fibroblasts are a novel way to observe cell proliferation across a scaffold. Their use for live imaging of cells is becoming more prevalent since their first use in 2004 [43]. To compare tdTomatoes natural fluorescence of the cell's mitochondria to a well-known staining of the cell's actin with the green fluorescent protein (GFP) the area of the same fibroblasts on the FSG ECM, fluoresced at 620 nm and 570 nm, were compared. A T-test was performed and showed that the tdTomato and GFP fluorescence were not statistically significantly different. This shows that either method can be used for staining cells to obtaining cell area [44]. Utilizing both stains together can give a better overall cells morphology as seen in Fig. 9ai and 9bi.

However, the formaldehyde used in the GFP staining can cause the cells to shrivel and change the cell's morphology from its natural morphology in a biological environment. The additional step of dying the cells on the FSG ECM could potentially be avoided further lowering cost and saving time. As seen in Fig.8b the uniqueness of these tdTomato cells additionally allows for live imaging as the cells might not always need to be fixed as in the use of GFP.

### **3.11. Live Cell Imaging**

Live Imaging of the tdTomato mice fibroblasts on the FSG ECM was achieved as tdTomato naturally fluoresces [46,47]. Viewing these cells live gives a better image of how the cells interact in their biological environment on the FSG ECM Fig.8b and allows additional information to be obtained from the cells that is lost by harsh chemicals during dying [47,48]. Comparing the live tdTomato fibroblasts (Fig.8b) to the fixed cells (Fig.8a) the live cells are seen to be more elongated as the imaging was done dynamically rather than statically. Additionally, Fig.8b only shows one layer of the FSG ECM. The fixed cells in figure 8a are slightly out of proportion as they were mounted to a microscope slide and flattened. Flattening the FSG ECM allowed more visibility of cells through the ECM, which is a beneficial but viewing an uncompressed FSG ECM depicts a better image of the cells in their natural biological environment and also eliminates an additional step and cost of mounting slides.

## **4. Conclusion**

A low-cost, “green” fabrication of fish skin gelatin (FSG) nanofibrous extracellular matrix (ECM) was achieved at a high productivity rate by using alternating field

electrospinning (AFES) and thermal crosslinking of an as-spun product. A production rate of 12.6 g/h of nanofibrous ECM material has been achieved, which significantly exceeds the reported values for different spinning methods and still can be scaled up easily. The AFES method produced FSG ECMs that have fiber diameters in a 100–200 nm range with a narrow size distribution and good pore to surface ratio to provide a desired scaffold for cells to proliferate across. Thermal crosslinking has been shown to not cause any nanofiber morphology changes or deformation of the ECM while providing controlled degradation rates of the ECMs. The performance of AFES produced FSG ECMs is very sensitive to the changes in the composition of precursor solution. It has been shown that small modifications of the solvent (e.g., acetic acid addition) or polymer (e.g., carboxymethyl cellulose addition) strongly affect the density, degradation rates and cellular response of the fabricated ECMs without significant changes in fiber diameter and surface morphology. Overall, AFES fabricated FSG ECM shows promising results for a base biomaterial that is bioactive, biocompatible, and suitable for scale-up manufacturing.

### **Acknowledgements**

A.K. and M.A. were supported through the NSF-IRES awards (Grant #1558268 and #1852207)

### **Competing Interest Statement**

There are no financial or personal conflicts of interest.

## REFERENCES:

- [1] Gao X, Han S, Zhang R, Liu G, Wu J. Progress in electrospun composite nanofibers: composition, performance and applications for tissue engineering. *J Mater Chem B*. 2019;7(45):7075–89.
- [2] Frantz C, Stewart KM, Weaver VM. The extracellular matrix at a glance. *J Cell Sci*. 2010;123(24):4195–200.
- [3] Ghassemi Z, Slaughter G. Storage stability of electrospun pure gelatin stabilized with EDC/Sulfo-NHS. *Biopolymers*. 2018;109(9):e23232.
- [4] Silva KD, Kumar P, Choonara YE, Toit LC du, Pillay V. Three-dimensional printing of extracellular matrix (ECM)-mimicking scaffolds: A critical review of the current ECM materials. *J Biomed Mater Res A*. 2020;108(12):2324–50.
- [5] Huang T, Tu Z, Shanguan X, Sha X, Wang H, Zhang L, et al. Fish gelatin modifications: A comprehensive review. *Trends Food Sci Technol*. 2019;86:260–9.
- [6] Karim AA, Bhat R. Fish gelatin: properties, challenges, and prospects as an alternative to mammalian gelatins. *Food Hydrocoll*. 2009;23(3):563–76.
- [7] Lee KY, Mooney DJ. Hydrogels for Tissue Engineering. *Chem Rev*. 2001;101(7):1869–80.
- [8] Ponticos M, Partridge T, Black CM, Abraham DJ, Bou-Gharios G. Regulation of Collagen Type I in Vascular Smooth Muscle Cells by Competition between Nkx2.5 and  $\delta$ EF1/ZEB1. *Mol Cell Biol*. 2004;24(14):6151–61.
- [9] Ghassemi Z, Slaughter G. Cross-linked electrospun gelatin nanofibers for cell-based assays. *Conf Proc Annu Int Conf IEEE Eng Med Biol Soc IEEE Eng Med Biol Soc Annu Conf*. 2018;2018:6088–91.

- [10] Gomes SR, Rodrigues G, Martins GG, Roberto MA, Mafra M, Henriques CMR, et al. In vitro and in vivo evaluation of electrospun nanofibers of PCL, chitosan and gelatin: A comparative study. *Mater Sci Eng C*. 2015;46:348–58.
- [11] Kwak HW, Shin M, Lee JY, Yun H, Song DW, Yang Y, et al. Fabrication of an ultrafine fish gelatin nanofibrous web from an aqueous solution by electrospinning. *Int J Biol Macromol*. 2017 ;102:1092–103.
- [12] Gomes SR, Rodrigues G, Martins GG, Henriques CMR, Silva JC. In vitro evaluation of crosslinked electrospun fish gelatin scaffolds. *Mater Sci Eng C*. 2013;33(3):1219–27.
- [13] Campiglio CE, Contessi Negrini N, Farè S, Draghi L. Cross-Linking Strategies for Electrospun Gelatin Scaffolds. *Materials*. 2019;12(15):2476.
- [14] Hickey RJ, Pelling AE. Cellulose Biomaterials for Tissue Engineering. *Front Bioeng Biotechnol*. 2019; 7: 45. 15.
- [15] Gómez-Guillén MC, Pérez-Mateos M, Gómez-Estaca J, López-Caballero E, Giménez B, Montero P. Fish gelatin: a renewable material for developing active biodegradable films. *Trends Food Sci Technol*. 2009;20(1):3–16.
- [16] Xie X, Chen Y, Wang X, Xu X, Shen Y, Khan A ur R, et al. Electrospinning nanofiber scaffolds for soft and hard tissue regeneration. *J Mater Sci Technol*. 2020;59:243–61.
- [17] Smith IO, Liu XH, Smith LA, Ma PX. Nanostructured polymer scaffolds for tissue engineering and regenerative medicine. *WIREs Nanomedicine Nanobiotechnology*. 2009;1(2):226–36.

- [18] Murphy CM, Haugh MG, O'Brien FJ. The effect of mean pore size on cell attachment, proliferation and migration in collagen–glycosaminoglycan scaffolds for bone tissue engineering. *Biomaterials*. 2010;31(3):461–6.
- [19] Loordhuswamy AM, Krishnaswamy VR, Korrapati PS, Thinakaran S, Rengaswami GDV. Fabrication of highly aligned fibrous scaffolds for tissue regeneration by centrifugal spinning technology. *Mater Sci Eng C*. 2014;42:799–807.
- [20] Haider A, Haider S, Rao Kummara M, Kamal T, Alghyamah A-AA, Jan Iftikhar F, et al. Advances in the scaffolds fabrication techniques using biocompatible polymers and their biomedical application: A technical and statistical review. *J Saudi Chem Soc*. 2020;24(2):186–215.
- [21] Xia L, Lu L, Liang Y, Cheng B. Fabrication of centrifugally spun prepared poly(lactic acid)/gelatin/ciprofloxacin nanofibers for antimicrobial wound dressing. *RSC Adv*. 2019;9(61):35328–35.
- [22] Jana H, Tomáš S, Monika Š, Marek P, Koš K. A comparison of the centrifugal force spinning and electrospinning of collagen under different conditions. *Proc. 8th Int. Conf. Nanomater. - Res. Appl*. 2016; 514–519.23.
- [23] Daristotle JL, Behrens AM, Sandler AD, Kofinas P. A Review of the Fundamental Principles and Applications of Solution Blow Spinning. *ACS Appl Mater Interfaces*. 2016;8(51):34951–63.
- [24] Medeiros ES, Glenn GM, Klamczynski AP, Orts WJ, Mattoso LHC. Solution blow spinning: A new method to produce micro- and nanofibers from polymer solutions. *J Appl Polym Sci*. 2009;113(4):2322–30

- [25] Liu F, Türker Saricaoglu F, Avena-Bustillos RJ, Bridges DF, Takeoka GR, Wu VCH, et al. Preparation of Fish Skin Gelatin-Based Nanofibers Incorporating Cinnamaldehyde by Solution Blow Spinning. *Int J Mol Sci*. 2018 Feb 22;19(2):618
- [26] Vilches JL, Souza Filho M de SM de, Rosa M de F, Sanches AO, Malmonge JA, Vilches JL, et al. Fabrication of Fish Gelatin Microfibrous Mats by Solution Blow Spinning. *Materials Research*. 2019; 22(suppl. 1): e20190158
- [27] Beishenaliev A, Lim SS, Tshai KY, Khiew PS, Moh'd Sghayyar HN, Loh H-S. Fabrication and preliminary in vitro evaluation of ultraviolet-crosslinked electrospun fish scale gelatin nanofibrous scaffolds. *J Mater Sci Mater Med*. 2019;30(6):62.
- [28] Nemati S, Kim S, Shin YM, Shin H. Current progress in application of polymeric nanofibers to tissue engineering. *Nano Converg* 2019; 6: 36 29.
- [29] Courtenay JC, Sharma RI, Scott JL. Recent Advances in Modified Cellulose for Tissue Culture Applications. *Molecules*. 2018;23(3):654.
- [30] Barati F, Farsani AM, Mahmoudifard M. A promising approach toward efficient isolation of the exosomes by core-shell PCL-gelatin electrospun nanofibers. *Bioprocess Biosyst Eng*. 2020;43(11):1961–71.
- [31] Pankongadisak P, Tsekoura E, Suwantong O, Uludağ H. Electrospun gelatin matrices with bioactive pDNA polyplexes. *Int J Biol Macromol*. 2020;149:296–308.
- [32] Lawson C, Stanishevsky A, Sivan M, Pokorny P, Lukáš D. Rapid fabrication of poly( $\epsilon$ -caprolactone) nanofibers using needleless alternating current electrospinning. *J Appl Polym Sci* 2016;133(13):43232
- [33] Pokorny P, Kostakova E, Sanetnik F, Mikes P, Chvojka J, Kalous T, et al. Effective AC needleless and collectorless electrospinning for yarn production. *Phys Chem Chem Phys*. 2014;16(48):26816–22.

- [34] Stanishvsky A, Tchernov J. Mechanical and transport properties of fibrous amorphous silica meshes and membranes fabricated from compressed electrospun precursor fibers. *J Non-Cryst Solids*. 2019;525.
- [35] Jirkovec R, Kalous T, Brayer WA, Stanishvsky AV, Chvojka J. Production of gelatin nanofibrous layers via alternating current electrospinning. *Mater Lett*. 2019;252:186–90.
- [36] Drews AM, Cademartiri L, Whitesides GM, Bishop KJM. Electric winds driven by time oscillating corona discharges. *J Appl Phys*. 2013;114(14):143302.
- [37] Kwak HW, Park J, Yun H, Jeon K, Kang D-W. Effect of crosslinkable sugar molecules on the physico-chemical and antioxidant properties of fish gelatin nanofibers. *Food Hydrocoll*. 2021;111:106259.
- [38] Gomes SR, Rodrigues G, Martins GG, Henriques CMR, Silva JC. In vitro evaluation of crosslinked electrospun fish gelatin scaffolds. *Mater Sci Eng C*. 2013;33(3):1219–27.
- [39] Chandra MV, Shamasundar BA, Kumar PR. Visco-Elastic and Flow Properties of Gelatin from the Bone of Freshwater Fish (*Cirrhinus mrigala*). *J Food Sci*. 2013;78(7):E1009–16.
- [40] Heyns JD, Ahmed Mohamed ET, Declercq NF. Non-linear ultrasonic and viscoelastic properties of gelatine investigated in the temperature range of 30 °C–60 °C. *Phys Fluids*. 2021;33(2):022002.
- [41] Hu W-W, Yu H-N. Coelectrospinning of chitosan/alginate fibers by dual-jet system for modulating material surfaces. *Carbohydr Polym*. 2013;95(2):716–27.

- [42] Liguori A, Uranga J, Panzavolta S, Guerrero P, de la Caba K, Focarete ML. Electrospinning of Fish Gelatin Solution Containing Citric Acid: An Environmentally Friendly Approach to Prepare Crosslinked Gelatin Fibers. *Materials*. 2019;12(17):2808.
- [43] Goudarzi Z M., Behzad, T, Ghasemi-Mobarakeh, L, Kharaziha, M., Enayati, MS, Structural and mechanical properties of fibrous poly (caprolactone)/gelatin nanocomposite incorporated with cellulose nanofibers. *Polymer Bulletin*. 2020; 77(2):717–40.
- [44] Paulett K, Brayer WA, Hatch K, Kalous T, Sewell J, Liavitskaya T, Vyazovkin S, Liu F, Lukáš D, Stanishevsky A. Effect of nanocrystalline cellulose addition on needleless alternating current electrospinning and properties of nanofibrous polyacrylonitrile meshes. *J. Appl. Polym. Sci*. 2018; 135 (5); 45772.
- [45] Gibson LJ, Ashby MF, Cellular solids: structure and properties, Second ed., Cambridge University Press, Cambridge, UK, 1997.
- [46] Syverud BC, Gumucio JP, Rodriguez BL, Wroblewski OM, Florida SE, Mendias CL, et al. A Transgenic tdTomato Rat for Cell Migration and Tissue Engineering Applications. *Tissue Eng Part C Methods*. 2018;24(5):263–71.
- [47] Prusicki MA, Balboni M, Sofroni K, Hamamura Y, Schnittger A. Caught in the Act: Live-Cell Imaging of Plant Meiosis. *Front Plant Sci*.2021;12.
- [48] Prusicki MA, Balboni M, Sofroni K, Hamamura Y, Schnittger A. Caught in the Act: Live-Cell Imaging if Plant Meiosis. *Front Plant Sci*. 2021;12.

## FIGURE CAPTIONS

Figure 1. Process of creating and *in-vitro* testing the FSG biomaterial. (a) The FSG precursor has a consistency of syrup. (b) The AFES process, (iv) electrode that the (iii) FSG precursor is placed on. After creating a potential difference in the FSG precursor (ii) nanofibers are lifted by ionic winds and initial impulse of the created fibers to the (i) collector which rotates collecting sheets of (c) nanofibers. (c.i.) A similar morphology to the ECM can be seen with an SEM image. (d) After confirmation, the nanofibers thermally crosslinked in an oven. After sterilization (e) *in-vitro* seeding of tdTomato fibroblasts confirms that the FSG is a viable biomaterial with (e.i.) cell growth.

Figure 2. SEM images and distribution of nanofiber diameters before thermal crosslinking and after thermal crosslinking. Before thermal crosslinking are (a) FSG (b) FSGAA-10 (c) FSGAA-5 (d) FSG/CEL-5. Histogram of uniform nanofiber diameters after thermal crosslinking where visible shrinkage in fiber diameter can be observed by the peaks shifting left. A side effect of thermal crosslinking was causing more uniform fiber diameters seen by the peak being skewed to the middle (e) FSG (f) FSGAA-10 (g) FSGAA-5 (h) FSG/CEL-5

Figure 3. Average fiber diameters of the different scaffolds comparing non-crosslinked to thermally crosslinked scaffolds. FSG, FSGAA-5, FSG/CEL-5 nanofiber diameters all shrank axially, while FSGAA-10 indicated a lateral increase in fiber diameters.

Figure 4. Density histograms of the nanofiber sheets showing a uniform distribution over different cross sections of the sheet. The peak of each histogram normally lies at the same density except for (a) FSG nanofiber which indicate a higher density for crosslinking at 160°C for 8 hours due to FSG non-Newtonians nature. The other nanofiber sheets (b) FSGAA-10 (c) FSGAA-5 and (d) FSG/CEL show a normal distribution for all crosslinking procedures around the same density.

Figure 5. Percent of mass retained of the whole scaffold for varying thermal crosslinking procedures. The nanofiber scaffolds were thermal crosslinked at (a) 180°C for 4 hours (b) 160°C for 4 hours and (c) 160°C for 8 hours. The samples thermally crosslinked at 160°C for 8 hours retained the most mass, and the addition of cmCEL made the nanofiber scaffold retain even more mass than the pure FSG nanofiber scaffold.

Figure 6. (a) FTIR Spectrum comparing the molecular structure before crosslinking, after crosslinking, and after sterilization. There is some oxidation in the band region around 1700 cm<sup>-1</sup> after UV sterilization. The degradation is small and not concerning. (b) FTIR Spectrum comparing the molecular structure between the varying nanofiber composition in Table 1 and 2. All spectra show the same trend except FSG/CEL 5 and 10 have a cellulose band in the 1000 cm<sup>-1</sup> region.

Figure 7. Proliferation and healthy cell growth across the varying scaffolds from Table 1 and 2. (a) The scaffolds with 0.5% cmCEL had the largest confluence. (b) the FSGAA-5 scaffold showed a higher cell confluence. This scaffold held the same nanofiber composition as the FSG/CEL-5 without the additional 0.5% cmCEL (c) These 5% cmCEL scaffolds had the largest area of cells (d) compared to the FSGAA-5

Figure 8. (a) Fluorescence images of fixed tdTomato fibroblasts proliferation across the

varying ECM compositions: (a.i.) FSG (a.ii.) FSG/CEL-5 (a.iii.) FSG/CEL-1 (a.iv.) FSGAA-5 (a.v.) FSGAA-10 (a.vi.) FSGAA-15. The difference in the cell proliferation between the ECM with cmCEL compared to those without can strongly be seen between (a.iii.) and (a.vi.). (b) Fluorescence images of live TdTomato fibroblasts proliferation across the varying ECM compositions: (b.i.) FSG (b.ii.) FSG/CEL-5 (b.iii.) FSG/CEL-1 (b.iv.) FSGAA-5 (b.v.) FSGAA-10 (b.vi.) FSGAA-15. The individual nanofiber strands with cells proliferating across the ECM can be seen best in (b.ii.) and (b.iv.)

Figure 9. (a) Composite fluorescence image of (i) FSG/Cell-1 ECM in comparison with only (ii) GFP fluorescence and (iii) tdTomato natural fluorescence of the fibroblasts; (b) Composite fluorescence image at  $\times 400$  of (i) FSGAA-5 ECM in comparison with only (ii) the GFP fluorescence of the cell's actin and (iii) the tdTomato fluorescence of the mitochondrial

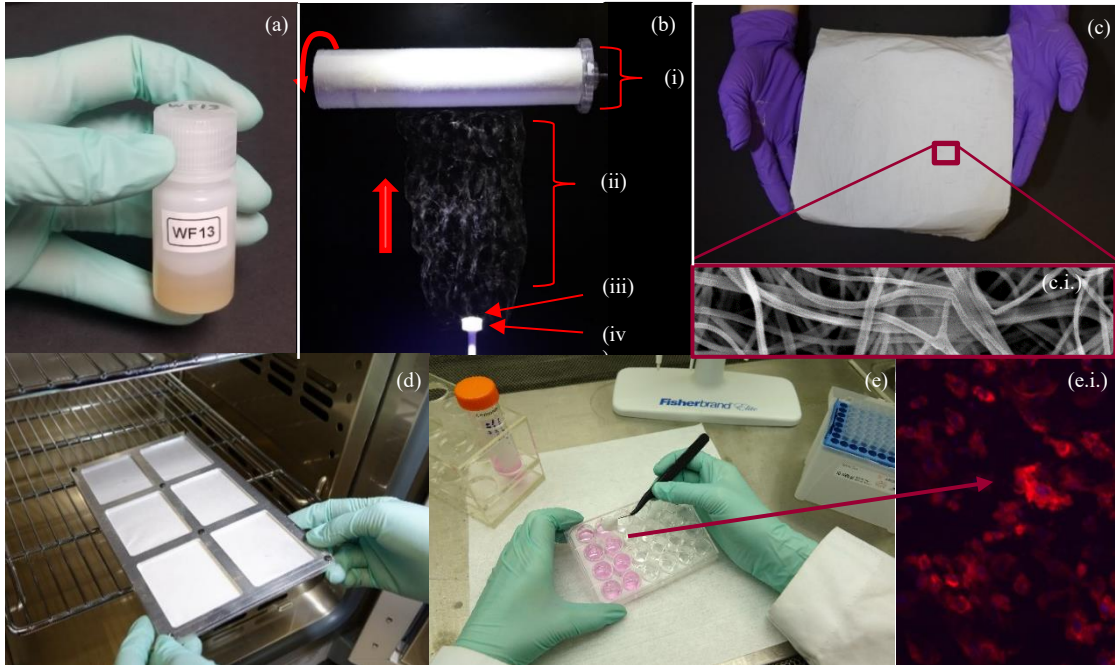


Figure 1: Process of creating and *in-vitro* testing the FSG biomaterial. (a) The FSG precursor has a consistency of syrup. (b) The AFES process, (iv) electrode that the (iii) FSG precursor is placed on. After creating a potential difference in the FSG precursor (ii) nanofibers are lifted by ionic winds and initial impulse of the created fibers to the (i) collector which rotates collecting sheets of (c) nanofibers. (c.i.) A similar morphology to the ECM can be seen with an SEM image. (d) After confirmation, the nanofibers thermally crosslinked in an oven. After sterilization (e) *in-vitro* seeding of tdTomato fibroblasts confirms that the FSG is a viable biomaterial with (e.i.) cell growth.

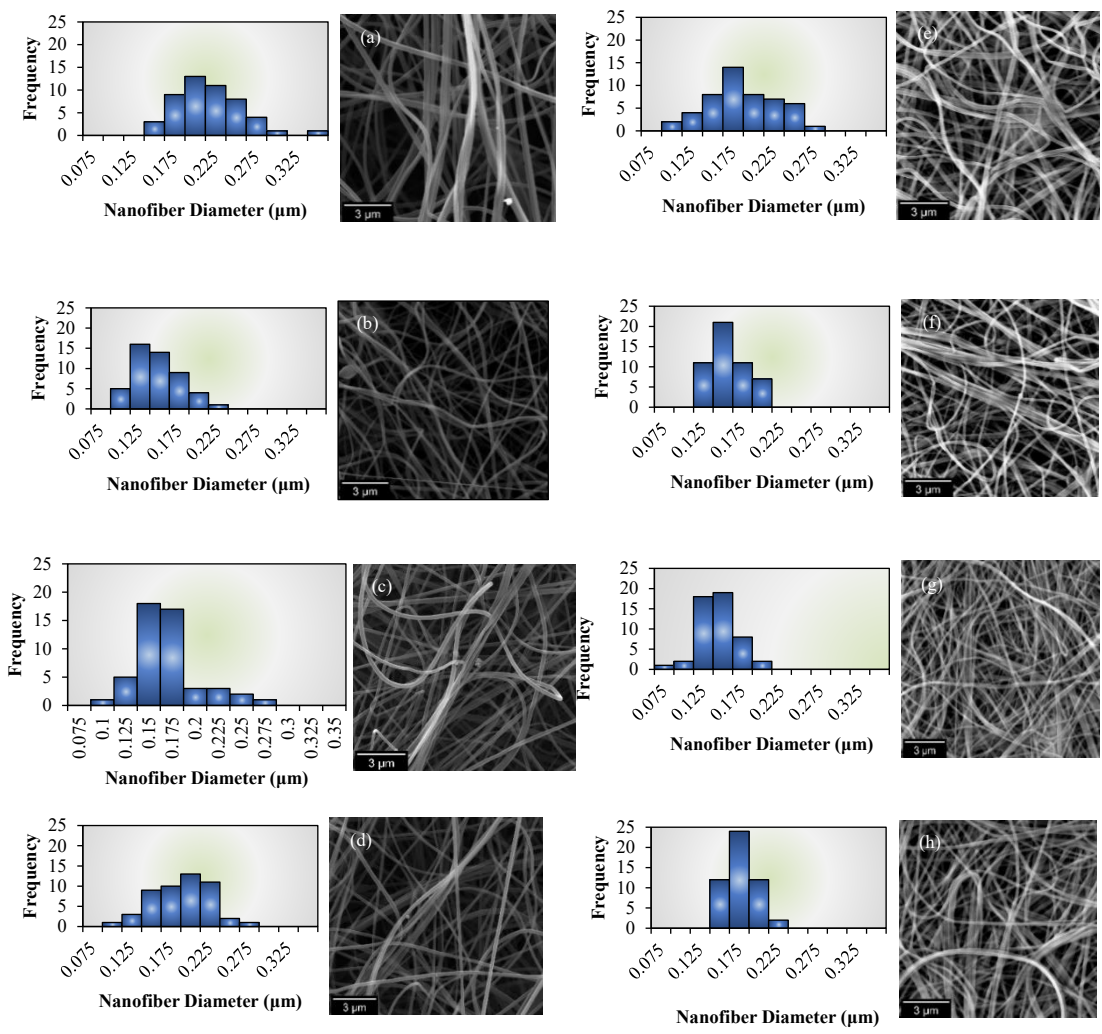


Figure 2: SEM images and distribution of nanofiber diameters before thermal crosslinking and after thermal crosslinking. Before thermal crosslinking are (a) FSG (b) FSGAA-10 (c) FSGAA-5 (d) FSG/CEL-5. Histogram of uniform nanofiber diameters after thermal crosslinking where visible shrinkage in fiber diameter can be observed by the peaks shifting left. A side effect of thermal crosslinking was causing more uniform fiber diameters seen by the peak being skewed to the middle (e) FSG (f) FSGAA-10 (g) FSGAA-5 (h) FSG/CEL-5  
2-column fitting image

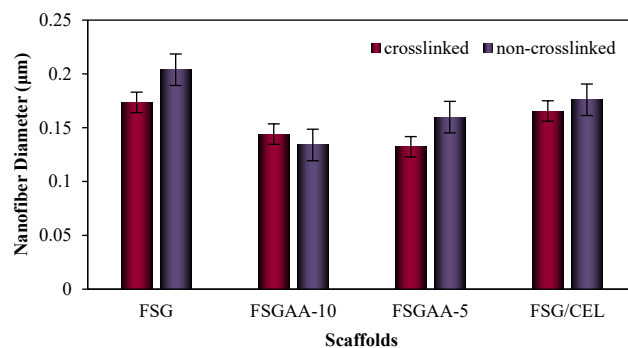


Figure 3: Average fiber diameters of the different scaffolds comparing non-crosslinked to thermally crosslinked scaffolds. FSG, FSGAA-5, FSG/CEL-5 nanofiber diameters all shrank axially, while FSGAA-10 indicated a lateral increase in fiber diameters.

Single column fitting image

Single column fitting image

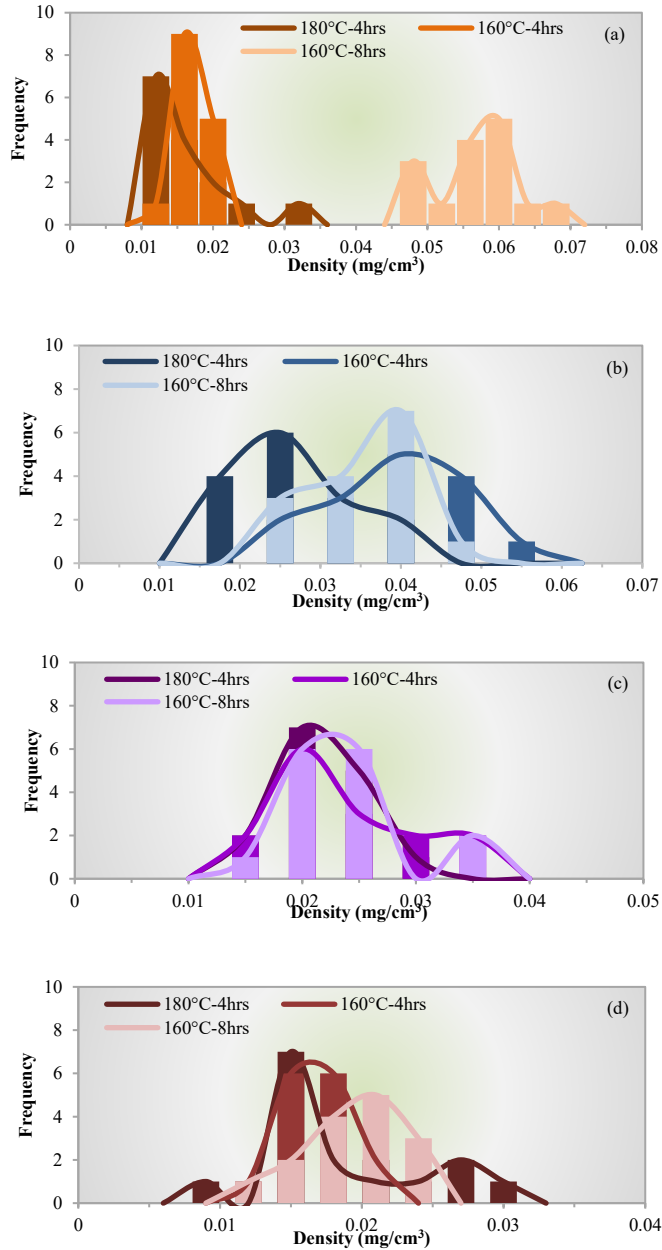


Figure 4: Density histograms of the nanofiber sheets showing a uniform distribution over different cross sections of the sheet. The peak of each histogram normally lies at the same density except for (a) FSG nanofiber which indicate a higher density for crosslinking at 160°C for 8 hours due to FSG non-Newtonian nature. The other nanofiber sheets (b) FSGAA-10 (c) FSGAA-5 and (d) FSG/CEL show a normal distribution for all crosslinking procedures around the same density.

Single column fitting image

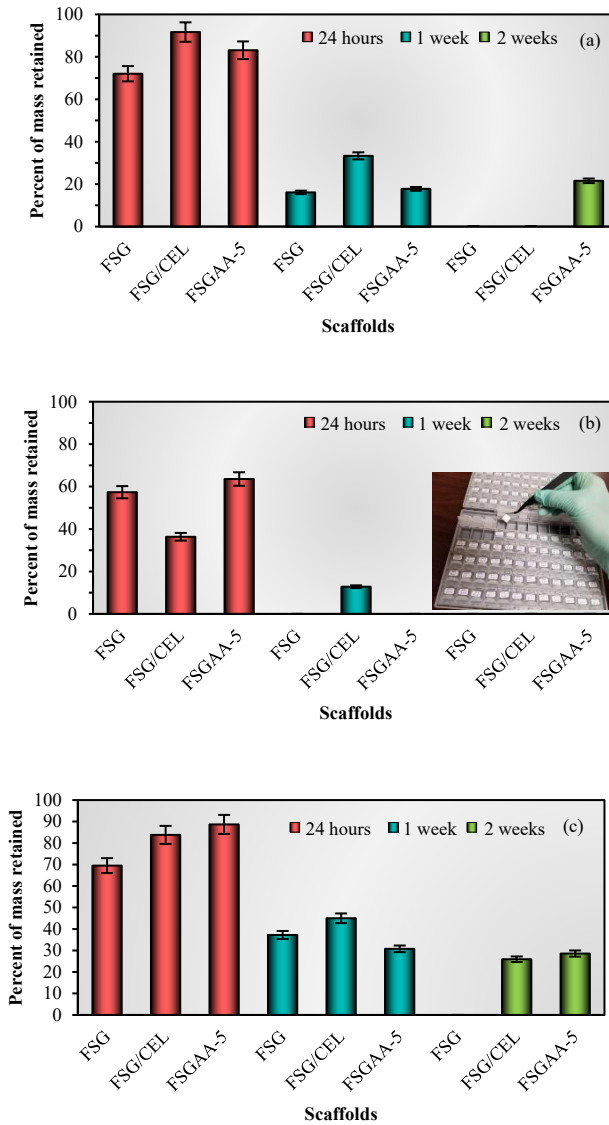


Figure 5: Percent of mass retained of the whole scaffold for varying thermal crosslinking procedures. The nanofiber scaffolds were thermal crosslinked at (a) 180°C for 4 hours (b) 160°C for 4 hours and (c) 160°C for 8 hours. The samples thermally crosslinked at 160°C for 8 hours retained the most mass, and the addition of cmCEL made the nanofiber scaffold retain even more mass than the pure FSG nanofiber scaffold.  
Single column fitting image

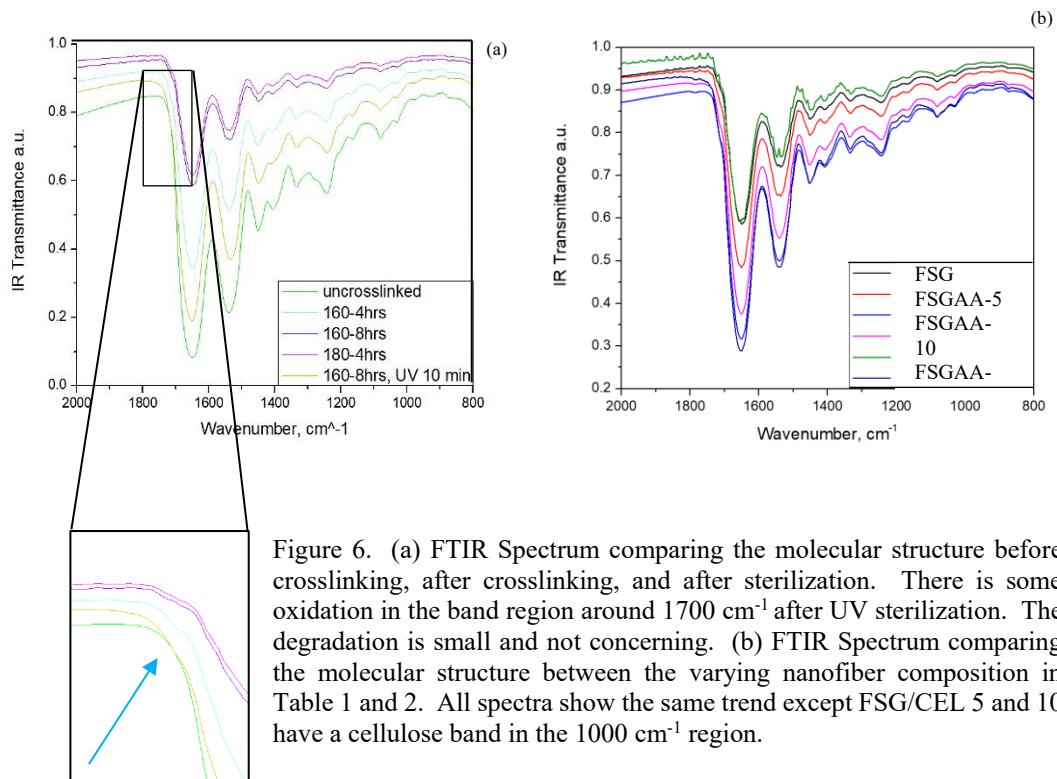


Figure 6. (a) FTIR Spectrum comparing the molecular structure before crosslinking, after crosslinking, and after sterilization. There is some oxidation in the band region around  $1700\text{ cm}^{-1}$  after UV sterilization. The degradation is small and not concerning. (b) FTIR Spectrum comparing the molecular structure between the varying nanofiber composition in Table 1 and 2. All spectra show the same trend except FSG/CEL 5 and 10 have a cellulose band in the  $1000\text{ cm}^{-1}$  region.

2-column fitting image

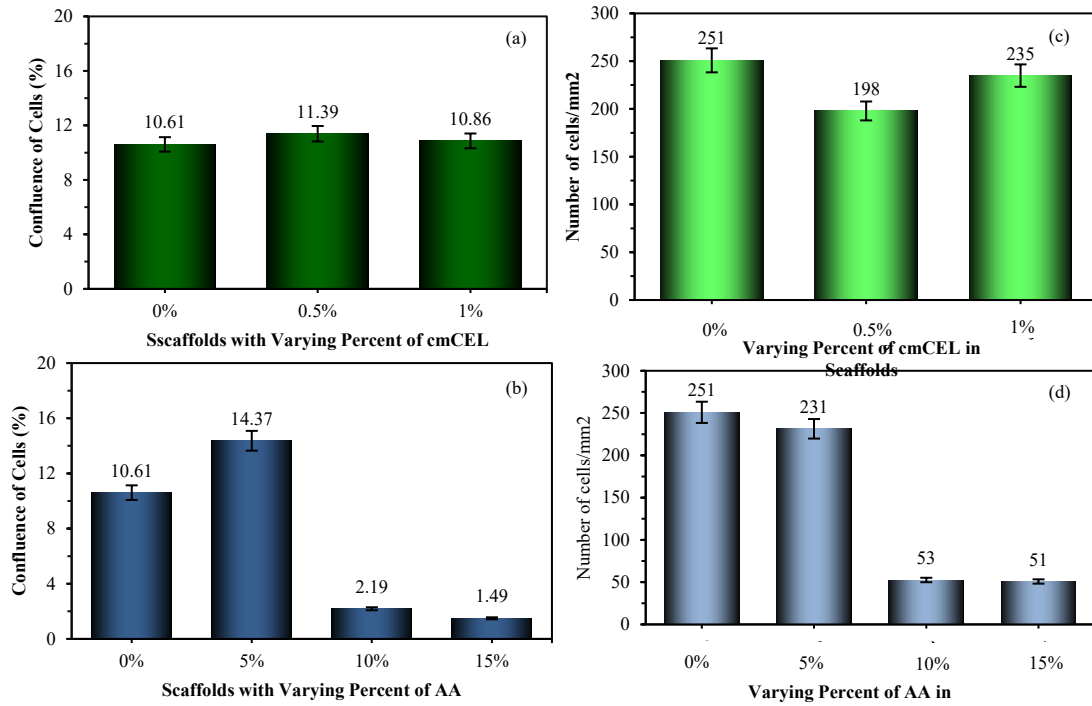


Figure 7: Proliferation and healthy cell growth across the varying scaffolds from Table 1 and 2. (a) The scaffolds with 0.5% cmCEL had the largest confluence. (b) the FSGAA-5 scaffold showed a higher cell confluence. This scaffold held the same nanofiber composition as the FSG/CEL-5 without the additional 0.5% cmCEL (c) These 5% cmCEL scaffolds had the largest area of cells (d) compared to the FSGAA-5

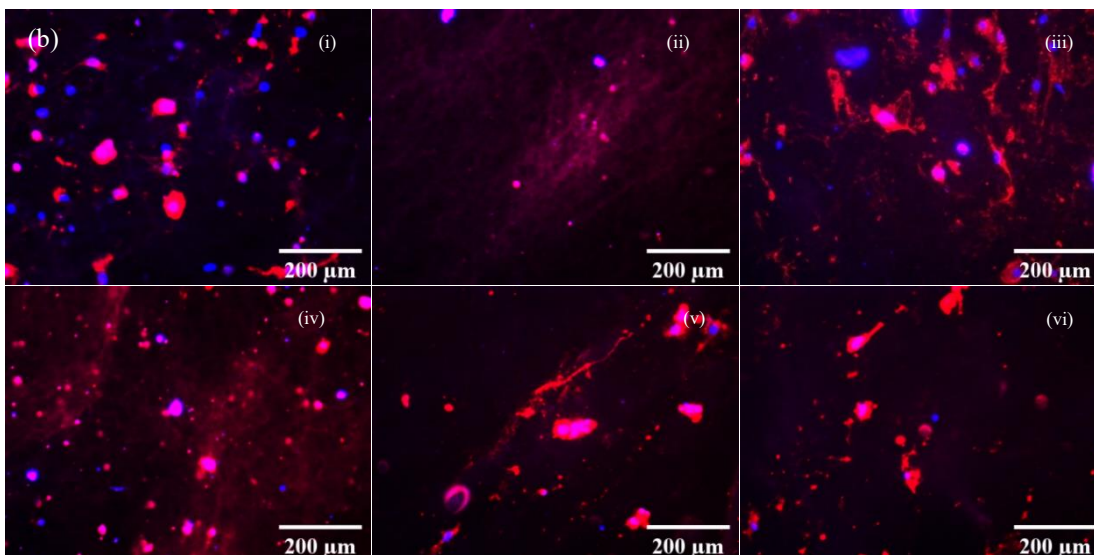
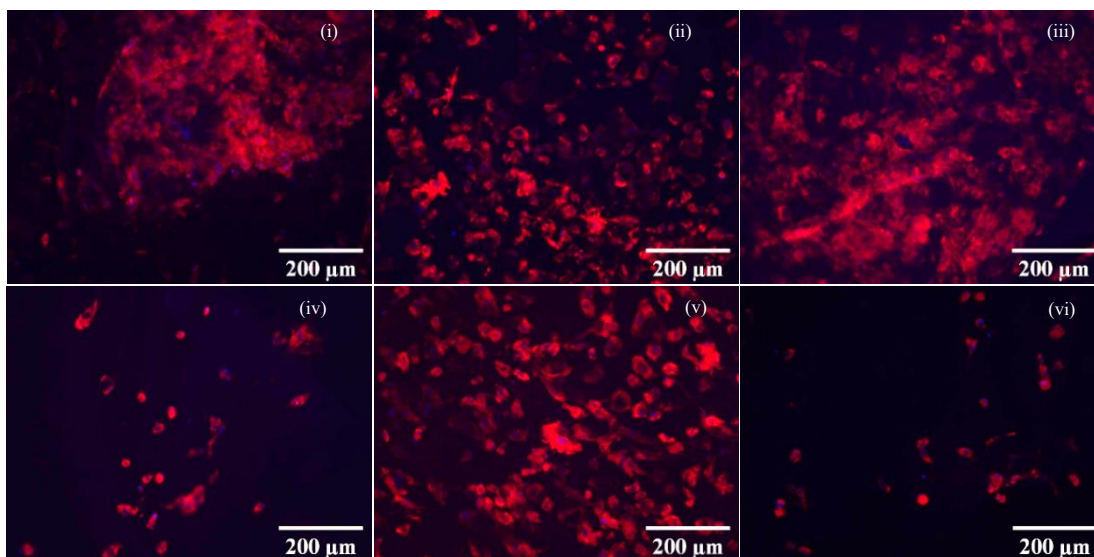


Figure 8: (a) Fluorescence images of fixed tdTomato fibroblasts proliferation across the varying ECM compositions: (a.i.) FSG (a.ii.) FSG/CEL-5 (a.iii.) FSG/CEL-1 (a.iv.) FSGAA-5 (a.v.) FSGAA-10 (a.vi.) FSGAA-15. The difference in the cell proliferation between the ECM with cmCEL compared to those without can strongly be seen between (a.iii.) and (a.vi.). (b) Fluorescence images of live TdTomato fibroblasts proliferation across the varying ECM compositions: (b.i.) FSG (b.ii.) FSG/CEL-5 (b.iii.) FSG/CEL-1 (b.iv.) FSGAA-5 (b.v.) FSGAA-10 (b.vi.) FSGAA-15. The individual nanofiber strands with cells proliferating across the ECM can be seen best in (b.ii.) and (b.iv.)

2-column fitting image

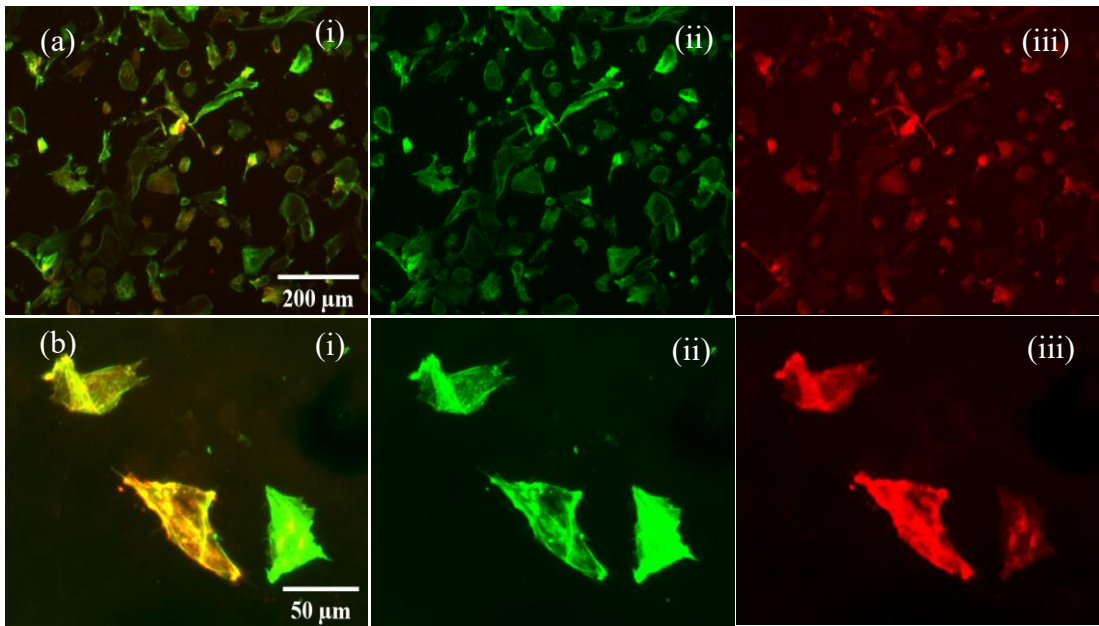


Figure 9: (a) Composite fluorescence image of (i) FSG/Cell-1 ECM in comparison with only(ii) GFP fluorescence and (iii) tdTomato natural fluorescence of the fibroblasts; (b) Composite fluorescence image at  $\times 400$  of(i) FSGAA-5 ECM in comparison with only (ii) the GFP fluorescence of the cell's actin and (iii) the tdTomato fluorescence of the mitochondrial

2-column fitting image

**Table 1.** Precursor compositions for pure FSG nanofiber with varying amounts of AA.

| <b>Materials</b>  | <b>FSG (wt%)</b> | <b>FSGAA-5<br/>(wt%)</b> | <b>FSGAA-10<br/>(wt%)</b> | <b>FSGAA-15<br/>(wt%)</b> |
|-------------------|------------------|--------------------------|---------------------------|---------------------------|
| FSG               | 31               | 31                       | 31                        | 31                        |
| dH <sub>2</sub> O | 69               | 65.6                     | 62.1                      | 58.6                      |
| AA                | -                | 4                        | 6.9                       | 10.3                      |

**Table 2.** Precursor compositions of FSG nanofibers with varying amounts of cmCEL.

| <b>Materials</b>  | <b>FSG (wt%)</b> | <b>FSG/CEL<br/>5 (wt%)</b> | <b>FSG/CEL<br/>1 (wt%)</b> |
|-------------------|------------------|----------------------------|----------------------------|
| Cellulose         | -                | 0.3                        | .3                         |
| FSG               | 31               | 31                         | 31                         |
| dH <sub>2</sub> O | 69               | 65.3                       | 58.4                       |
| AA                | -                | 3.4                        | 10.3                       |

**Table 3.** Young's moduli of fish gelatin based nanofibrous scaffolds tested under tensile load after the exposure in SBF for 1 and 3 days.

| <b>Exposure<br/>Time, h</b> | <b>Young's Modulus, kPa</b> |                  |                |                 |
|-----------------------------|-----------------------------|------------------|----------------|-----------------|
|                             | <b>FSG</b>                  | <b>FSG/CEL-5</b> | <b>FSGAA-5</b> | <b>FSGAA-10</b> |
| 24 h                        | 5.6±1.4                     | 32.8±3.4         | 12.1±2.2       | 21.1±2.9        |
| 72 h                        | 0.52±0.2                    | 23.8±3.1         | 9.0±1.7        | 17.7±2.6        |

DEGRADATION BEHAVIOR AND VISCOELASTIC  
PROPERTIES OF ELECTROSPUN FISH SKIN GELATIN-BASED  
NANOFIBROUS SUBSTRATE IN BIOLOGICAL ENVIRONMENT

by

AMANDA KENNEL, OLIVIA SHIVERS, SARAH NEALY, RANOAH  
CHATTERTON, ANDREI STANISHEVSKY

In preparation for *Journal of the Mechanical Behavior of Biomedical Materials*

Format adapted for dissertation

Degradation Behavior and Viscoelastic Properties of Electrospun Fish Skin Gelatin-based Nanofibrous Substrate in Biological Environment

Amanda Kennell<sup>a\*\*</sup>, Olivia Shivers<sup>a</sup>, Sarah Nealy<sup>b</sup>, Ranoah Chatterton<sup>a</sup>, Andrei Stanishevsky<sup>a</sup>

<sup>a</sup> *Department of Physics, University of Alabama at Birmingham, Birmingham, Al 35294, USA*

<sup>b</sup> *Department of Chemistry, University of Alabama at Birmingham, Birmingham, Al 35294, USA*

## **Highlights**

- Fabrication of fish skin gelatin material
- Controlled degradation with crosslinking
- Viscoelastic properties show strain hardening

## **Abstract**

As cardiovascular diseases are a leading cause of death globally there is a urgent call for a tissue engineered natural vascular material replacement. This paper presents an innovative fish skin gelatin-based nanofibrous extracellular matrix (ECM) with polysaccharides that has a controllable degradation rate and mechanically viable properties for vascular tissue. Fabrication of the ECM came through an uncommon electrohydrodynamic process of Alternating Field Electrospinning that is scale-up. The ECM underwent various post-processing treatments of freeze drying, thermal, glutaraldehyde vapor, and sugar enhanced thermal crosslinking. Resulting in almost full degradation at one week with 9.8% mass retention or retaining as much as 89.3% mass after one week in a physiological environment. The stress-strain curves for the ECM in a physiological environment mimicked strain-hardening found in normal body tissue with and elastic moduli as high as  $64.9 \pm 7.6$  kPa after degrading in a physiological environment for 24hrs. This fish skin gelatin-based nanofibrous ECM mimicked ideal properties for vascular tissue with a scale-up fabrication method.

**Key words:** Fish Skin Gelatin, Alternating Field Electrospinning, Crosslinking, Biodegradable, Viscoelastic

**Funding:** No funding was associated with this paper

**Conflicts of interest/ Competing interests:** Not applicable

**Availability of data and material:**

**Author Contributions:**

Amanda Kennell—Conceptualization; Data curation; Formal analysis, Methodology, Validation, Roles/Writing—original draft; Writing - review & editing

Olivia Shivers—Data curation

Sarah Nealy—Data curation, Formal analysis, Roles/Writing - original draft

Ranoah Chatterton—Data curation

Andrei Stanishevsky—Conceptualization, Formal analysis, Writing - review & editing

**Consent for publication:** All the authors give their consent to the journal to publish this article.

## 1. Introduction

Mass producing a natural tissue to replace vascular material would drastically affect change in cardio vascular diseases which are a leading cause of deaths (Powell-Wiley et al., 2021). A natural vascular tissue must retain similar properties to the body's vascular tissue. Several key components being the ability to mimic the body's extracellular matrix in morphology and composition, to degrade at a controlled rate for wound healing, and to have an elastic modulus similar to vascular tissue.

Fabricating a natural vascular tissue to mimic the body's tissue is done through construction of an extracellular matrix (ECM) (Rahmati et al., 2021). This ECM has a random fiber morphology with fiber diameters on the order of 50 to 500nm (Smith et al., 2009). A promising fabrication technique called electrospinning can closely mimic the bodies ECM morphology and produce fiber diameters ranging from 100-1100nm with a healthy surface area to pore ratio for cell proliferation (Chen et al., 2022; Rahmati et al., 2021).

The body's ECM fiber composition consists largely of collagen (Ghassemi and Slaughter, 2018; Soliman et al., 2022). Fabrication of collagen nanofibers is difficult and can require harsh solvents driving up cost. An alternative to collagen which is also a derivative of collagen is gelatin. Gelatin is naturally biocompatible (González-Ulloa et al., 2023) biodegradable (Chiulan et al., 2021; Kennell et al., 2022) and simpler to work with. Specifically gelatin from fish skin which additionally is more ethically kosher than type A and B gelatin (Huang et al., 2019; Soliman et al., 2022).

Gelatin is a natural viscoelastic material (Warner et al., 2019) with poor mechanical properties (González-Ulloa et al., 2023) but good elasticity. FSG has lower mechanical

properties than mammalian gelatin but is less expensive and safer (Soliman et al., 2022). To enhance FSG mechanical properties, other polymers can be added. Combining FSG with sodium carboxymethyl cellulose, a polysaccharide that naturally has good mechanical properties and is biodegradable (Kanikireddy et al., 2020), and chitosan, another polysaccharide that is biocompatible and antimicrobial (Felt et al., 1998; Methods of Chitosan Identification, 2022), can enhance FSG mechanical strength and biocompatibility for use as vascular tissue.

Further enhancement of the NF FSG material comes through crosslinking. Crosslinking mechanically strengthens and prevents dissolution of gelatin NF material in a fluid environment. The most common crosslinking technique for NF electrospun materials and gelatin materials is chemical vapor crosslinking (Skopinska-Wisniewska et al., 2021) with Glutaraldehyde (GTA) (Kwak et al., 2021; Lim, 2022). GTA crosslinking covalently bonds linear polymers together (Noble et al., 1999; Pellá et al., 2018), improving mechanical strength and slowing the material's degradation rate (Lim, 2022, p. 20). GTA, however, is toxic to cells and must be removed causing an extra procedure (Kwak et al., 2021; Pellá et al., 2018). In contrast to GTA, thermal crosslinking mechanically strengthens a material without use of harsh solvents (Gungor et al., 2021). However, thermally crosslinked material degrades rapidly and needs to be combined with another crosslinking technique (Kennell et al., 2022). An alternative crosslinking method is an environmentally safe technique of combining sugar with thermal crosslinking. Sugar enhanced thermal crosslinking causes a Maillard reaction, giving stability to the mechanical and degradable properties of a FSG material (Kwak et al., 2021).

The objective of this paper is to investigate a NF FSG material suitable for its degradation and mechanical properties as a natural vascular tissue platform. The NF material was made with a complex electrohydrodynamic technique called alternating field electrospinning which has the advantage mimicking an NF ECM material and making NF material scale-up for industry (Lacy et al., 2023; Persano et al., 2013; Pokorny et al., 2014). The NF FSG material has a controllable degradation rate resulting from various crosslinking procedures after fabrication. An in-depth study of the material's elasticity, Young's modulus which is the most important mechanical property for an ECM (C. Liu et al., 2023), in dry, wet, and wet degraded states will be discussed to verify its validity as a natural vascular tissue.

## **2 Materials and methods**

### *2.1 Starting materials*

Gelatin from cold water fish skin and chitosan (low molecular weight), both in powder form, were acquired from Sigma-Aldrich, and carboxymethyl cellulose sodium salt (CMC, viscosity 10–20 mPa·s in 2 wt% aqueous solution) also in powder form, was obtained from Scientific Polymer Products, Inc. The N-Acetyl-D-glucosamine (AGA, 98+%) and glutaraldehyde (GTA, reagent grade, 50 % w/w aqueous solution) were received from Alfa Aesar and Fisher Scientific, respectively. The in-house DI water ( $<2.0 \mu\text{S}\cdot\text{cm}^{-1}$ ) was used as a major solvent and acetic acid (AA, glacial, 99+%, Alfa Aesar) was used as an additional solvent.

## 2.2. Electrospinning precursor compositions

Fish gelatin (fGel) electrospinning precursor was prepared by dissolving fGel in DI water under stirring at room temperature. Chitosan and CMC additives were dissolved in a mixture of DI water and AA and added to fGel solution. The chitosan solution was initially heated to 37 °C for faster dissolution of this polysaccharide. The chosen precursor compositions listed in Table 1 were utilized in AFES process to prepare the fGel-based nanofibrous materials.

**Table 1:** Compositions of fGel precursors without and with additives of CMC (fCMC) and chitosan (fChit).

| <i>w/w</i>   | <b>dH<sub>2</sub>O</b> | <b>Acetic Acid</b> | <b>Additive</b> | <b>Fish Skin Gelatin</b> |
|--------------|------------------------|--------------------|-----------------|--------------------------|
| <i>fGel</i>  | 69.0                   | -                  | -               | 31.0                     |
| <i>fCMC</i>  | 58.2                   | 10.3               | 0.7             | 30.8                     |
| <i>fChit</i> | 51.4                   | 17.1               | 0.7             | 30.8                     |

A separate group of AFES precursors with the compositions listed in Table 1 was prepared with 10 wt% of AGA added with respect to the mass of polymer component of the precursor.

## 2.3. Alternating field electrospinning of fGel-based nanofibers

To establish the spinnability of the fGel precursors, they were pipetted onto the surface of a 12.5 mm diameter disk spinneret of the custom-built alternating field electrospinning (AFES) machine. The 27 kV rms AC voltage (60 Hz), which was determined to be the best for all precursors in this study, was applied to the spinneret. The multiple liquid jets were generated under the applied AC electric field from the layer of precursor on the spinneret

surface. Upon solvent evaporation those jets formed a uniform tubular flow of nanofibers propagating upward.

Once the spinnability was established, the precursors were delivered to a 25-mm diameter flat disk spinneret using a syringe pump to produce the nanofibrous sheets with typically  $\sim 30 \times 20$  cm<sup>2</sup> and thickness up to 1 mm by the collecting the nanofibers on a rotating, 10-cm diameter cylindrical plastic collector placed at 25–30 cm from the spinneret

#### *2.4. Post-processing and crosslinking of fGel-based nanofibrous material*

As spun nanofibrous sheets were removed from the AFES machine's collector and cut into small rectangular pieces with suitable dimensions to study their degradation rates and mechanical properties. Several approaches have been used for the post-processing of fGel-based nanofibers to study the effect of different factors on the fiber degradation rate in simulated body fluids (SBF). The approaches included the freeze-drying process to remove the residual water from as-spun nanofibers, thermal, common GTA crosslinking, and AGA enhanced thermal crosslinking in different combinations. Thermal crosslinking was performed at 160°C for 8 hours in a sterile oven (Heratherm, Thermo Scientific). Crosslinking with glutaraldehyde was carried out by placing the nanofibrous material on a plate in a chamber above a layer of GTA/water solution for 30 min. The various combinations of post-processing procedures are summarized in Table 2 and visualized in figure 1b.

**Table 2:** Post-processing procedures for fGel-based nanofibrous materials. Thermal crosslinking (T) was used in every case and freeze-drying (F) was use in the half of the tests. Letter G indicates glutaraldehyde crosslinking and AGA indicates the presence of glucosamine in the nanofibers.

|                  | Freeze<br>drying (F) | Thermal<br>Crosslink (T) | AGA+T<br>Crosslink (A) | Chemical Vapor<br>crosslinking (G) |
|------------------|----------------------|--------------------------|------------------------|------------------------------------|
| <i>FT</i>        | ✓                    | ✓                        | –                      | –                                  |
| <i>FTG-30m.</i>  | ✓                    | ✓                        | –                      | ✓                                  |
| <i>FTG.</i>      | ✓                    | ✓                        | –                      | ✓                                  |
| <i>FTA</i>       | ✓                    | ✓                        | ✓                      | –                                  |
| <i>FTAG-30m.</i> | ✓                    | ✓                        | ✓                      | ✓                                  |
| <i>FTAG</i>      | ✓                    | ✓                        | ✓                      | ✓                                  |
| <i>T</i>         | –                    | ✓                        | –                      | –                                  |
| <i>TG-30m.</i>   | –                    | ✓                        | –                      | ✓                                  |
| <i>TG</i>        | –                    | ✓                        | –                      | ✓                                  |
| <i>TA</i>        | –                    | ✓                        | ✓                      | –                                  |
| <i>TAG-30m.</i>  | –                    | ✓                        | ✓                      | ✓                                  |
| <i>TAG</i>       | –                    | ✓                        | ✓                      | ✓                                  |

### 2.5. Degradation tests of fGel-based nanofibrous material

For the degradation tests in simulated body fluid (SBF) (SIGMA, Dulbecco's Phosphate Buffered Saline, Sigma Aldrich), the fGel samples were placed in SBF for 1, 3 and 7 days. The samples were kept at normal body temperature of 37°C in a LabLine incubator. Every 48 hours the SBF in the samples was replaced with new SBF. The nanofibrous material was removed from the SBF after its designated time period. After removal from the SBF, the material was rinsed in DI water to remove any residual SBF. The samples were kept in a vacuum chamber until fully dried. After being fully dry, the samples were weighed using a precision balance with 0.1 mg resolution and the SBF-exposed fGel material weight was compared to the initial weight to observe mass retention.

### 2.6. Infrared spectroscopy of degraded fGel materials

Fourier Transform Infrared Spectroscopy (FTIR, Bruker Alpha ATR-FTIR spectrometer) was performed on the two best samples that showed most mass retention after one week in SBF and then their mimic sample without freeze drying. The Attenuated

Total Reflectance (ATR) accessory was used for signal enhancement of chemical species in sampling the small quantities of fGel nanofibrous materials. The number of scans was set to 32 with a resolution on  $4\text{ cm}^{-1}$  for all fGel materials. Scans of the fGel materials with the crosslinking procedures FTA, TA, FTG, and TG were taken after 1d and 7d in SBF at  $37^{\circ}\text{C}$ . All materials were dried before scanning.

### *2.7. Dry mechanical tests of nanofibrous materials*

Dry tensile tests were performed on each material (fGel, fCMC, and fChit) before and after the crosslinking procedure (Figure 1f,g). These samples had width of 3.2 mm and were run with a gauge length of 6 mm due to the limitation of the used tensile tester (ADMET eXpert 4000, 5 N force cell, 25 mm maximum motor shaft travel length). Thus, the sample dimensions were chosen based on the expected high elastic behavior of tested nanofibrous materials. A minimum of three samples were then run at a strain rate of 50% of the gauge length per minute for each sample. The high dry strain rate was chosen to compare the dry materials' elasticity to the elasticity of wet materials. The elastic modulus for the dry samples was taken from the linear elastic region on the stress-strain curve, figure 3, after comparison to the  $R^2$  to ensure the most linear region was used.

### *2.8 Wet Mechanical Tests of nanofibrous material*

The two crosslinking methods that withstood the highest stress with an appropriate Young's modulus in dry conditions were then tensely tested in Fetal Bovine Serum (FBS) at  $37^{\circ}\text{C}$  to simulate a bloodlike environment. The fGel, fCMC, fChit materials were crosslinked with the procedures FTA and FTG. Three of each type of samples were left in

fluid for 5 minutes and then 24 hours. The sample were tensely strained after both time periods in FBS at 37°C with the ADMET eXpert 4000 with the same parameters and sample dimensions as the dry tensile tests. The samples in fluid were stretched until breakage or to 21mm (around the limit of the ADMET eXpert 4000). Most of the samples did not break. The samples were analyzed exactly as the procedure for the dry samples, except the second linear region was chosen.

### *2.9. Porosity measurements*

The porosity for each of each fGel-based material before and after the crosslinking procedure was determined as

$$\varepsilon = (1 - d_{\text{sample}}/d_{\text{theor}}) \times 100\% \quad \text{Eq.(1)}$$

where  $d_{\text{sample}}$  was determined as the sample's mass divided by its volume, and  $d_{\text{theor}}$  is the density of bulk fish gelatin with the appropriate adjustments made for the additives. Each NF material with their set crosslinking procedure's density was then compared to bulk fish gelatin density to calculate the porosity of each. The fCMC and fChi materials underwent the same procedure.

## **3 Results and Discussion**

### *4.1 Fabricating FSG NF material with AFES*

Three different precursors, table 1, fGel, fCMC, fChi were optimized to make long continuous nanofibers by alternating field electrospinning (AFES). The neutral NFs

(Pokorny et al., 2014) were collected onto a rod making a long fluffy sheet of NFs, figure 1.a. The benefits of AFES NF material is the high production rate which can be scaled-up for industry (Pokorny et al., 2014). Additionally, FSG NF material has a production rate of 12.6g/h listed by Kennell et al (Kennell et al., 2022). Electrospinning, additionally, has the ability to strongly mimic the necessary extracellular matrix structure (ECM) needed for biomaterials (Chen et al., 2022; Rahmati et al., 2021) which made AFES the ideal technique to make fish skin gelatin (FSG) NF material.

#### *4.2 Controlling degradation rate through crosslinking*

A desired outcome from the NF FSG material was control of degradation rate. One way to control degradation rate of a material is through crosslinking or addition of other polymers. Table 2 shows twelve variations of three main crosslinking procedures. Thermal crosslinking (T) was utilized in every crosslinking combination as it cost efficient and environmentally safe. The other variations were AGA enhanced thermal crosslinking (TA), GTA vapor and thermal crosslinking (TG), and a post-processing procedure of freeze drying (FD).

In figure 2, T crosslinking only retains 9.8% of the fish skin gelatin (fGel) materials' mass which is not optimal for severe wounds. T crosslinking can be combined with other crosslinking procedures to still lower costs and remain "green" (Gomes et al., 2013). An ideal crosslinking combination for control of degradation, is gelatin with glutaraldehyde (GTA) crosslinking (cite). The fGel material crosslinked thermally and with GTA vapors had 60.1% mass retention after one week in synthetic body fluid (SBF). The slowed degradation rate comes from the amine groups from gelatin covalently bonding to

glutaraldehyde's aldehyde groups (G. Liu et al., 2023). Resulting in fGel with thermal and GTA vapor crosslinking (TG) showing better mass retention during hydrolysis (G. Liu et al., 2023; Mo et al., 2020) than just T crosslinking. A complication of GTA vapor crosslinking is only the surface material is crosslinked due to poor GTA vapor penetration (Dechojarassri et al., 2023). To promote more uniform bonding T crosslinking was enhanced with N-acetyl-D-glucosamine (AGA). AGA enhanced thermal crosslinking retained 78.3% mass after one week in SBF. AGA was evenly mixed and uniformly electrospun within the FSG NFs allowing uniform crosslinking. AGA enhanced T crosslinking (TA), additionally, causes the Maillard reaction with fGel during heat treatment. The AGA becomes a reducing sugar and creates a molecular bond to an amino group on gelatin. So fGel-TA had the largest mass retention.

A final procedure of freeze drying (FD) was combined with GTA vapor crosslinking and AGA enhanced thermal crosslinking. FD dehydrates a material by evaporating water from it at low pressure under 0°C conditions. As the fGel material is water based and GTA was 50wt% water, freeze drying removed excess water in the material to provide stronger bonding and prevent water swelling inside the material during hydrolysis. This resulted in FD fGel-TG having 90.2% mass retention after 1 week in SBF. That is 30.1% more mass retention than without FD. FD additionally benefitted TA crosslinking as FD fGel-TA material had higher mass retention of 85% after one week in SBF than with no FD.

Combining the two crosslinking procedures of GTA vapor and AGA enhanced thermal crosslinking did as well as or worse than the crosslinking procedures FTA and FTG which both retained the most mass of fGel after 1 week. Three T-tests were run on the FTG

and FTA crosslinking comparing mass retention after 1d, 3d, and 7d in SBF and the mass retention of both was not statistically different.

In total, Figure 2 shows the mass retention from 1 day to 1 week for each crosslinking procedure. Three one-way Anovas were run on the crosslinking procedures for 1d, 3d, and 7d in SBF. The crosslinking procedures were found to be statistically different in mass retention for each time period. These crosslinking methods can target a desired time period for the biomaterial to degrade within depending on wound severity. The electrospin FSG NF material allows for greater scale-up as a biomaterial since it can have a controlled degradation rate.

#### *4.3 FTIR analysis of nanofibrous fGel materials*

Infrared absorbance spectra of all as spun, crosslinked, and SBF exposed samples of fGel materials were essentially the same for all tested compositions and crosslinking procedures (Figure 3). The main features of FTIR spectra of as spun nanofibers (Fig.3a) are associated with fGel component and reveal two strong absorption bands at 1650 (Amide-I) and 1539  $\text{cm}^{-1}$  (Amide-II), followed by 1450 (CH<sub>2</sub>), 1407 (–COO), 1335 (CH<sub>2</sub>), 1242 (N–H coupled with N–C), 1080 (C–O) and 1030 (C–O)  $\text{cm}^{-1}$ . A broad absorption band centered at 3292  $\text{cm}^{-1}$  (Amide A) also shows shoulders due to absorbed and bound water, as well as small peaks at 3074 (Amide B), 2936 (CH<sub>2</sub>) (Zhang et al., 2005, Kudo and Nakashima, 2020).

The apparent positions of fGel peaks remained nearly the same after different types of the post-processing. The only exception was as spun fGel-AGA material where the small peaks due to infrared absorption bands of AGA at 1059 (mainly C–O

vibrations), 1105 (C–O), 1121 (C–C, C–H, C–N), 1312 and 1380 (C–H, O–H)  $\text{cm}^{-1}$  were observed (Fig.3a, middle). Besides, the apparent positions of Amide-I peak in fGel-AGA and Amide-II peak are shifted to 1648  $\text{cm}^{-1}$  and 1546  $\text{cm}^{-1}$ , respectively, from their corresponding positions at 1650  $\text{cm}^{-1}$  and 1539  $\text{cm}^{-1}$  in pristine fGel nanofibers. Those shifts can be caused by the overlaps with 1627 (primarily C=O) and 1550 (N–H and N–C)  $\text{cm}^{-1}$  absorption peaks in AGA (Kovács et al., 2008). However, thermal processing led to disappearance of AGA absorption peaks due to Maillard reaction (Dechojarassri et al., 2023) and crosslinking of fGel (Fig.3a, top). A weak absorption peak centered at 1712  $\text{cm}^{-1}$  appeared after T-crosslinking as a shoulder of Amide-I band due to the formation of the reaction intermediates with carbonyl groups. The degree of chemical interaction of fGel with chitosan and CMC was not resolved by FTIR due to small concentrations of those polysaccharide.

FTIR spectra acquired from the crosslinked samples after 1 day of SBF exposure followed by drying reveal up to 18–22  $\text{cm}^{-1}$  apparent shift of fGel Amide I, Amide II and Amide A peak positions to lower wavenumbers (Fig.3b) and smaller, 1–8  $\text{cm}^{-1}$  downshifts of most other peaks. The observed shifts were apparently the same for all tested samples regardless the sample composition and post-processing technique used (Fig.3b). This trend remained after 7 days of SBF exposure (Fig.3c). The observed shifts are likely associated with the changes in fGel secondary structure and peak intensity rearrangement during the amide protonation when exposed to SBF (Polyak and Reich, 2019), (Prystupa and Donald, 1996).

#### *4.4.1 Electrospun FSG NF mechanical behavior*

To be a candidate for vascular tissue the NF FSG electrospun material must behave similar to vascular tissue's mechanical properties in a physiological environment. Gelatin is a viscoelastic material similar to body tissue (cite). When gelatin is strained, its elastic component allows the NF to retain their shape. Once strained passed the elastic region, gelatins viscous component takes over causing permanent deformation (cite). The elasticity region is focused on in this paper. Once the electrospun NF FSG material losses its elasticity, it is no longer a candidate for vascular tissue.

Figure 3.a shows the stress-strain curves that were obtained after tensely straining the material in table 1 with no crosslinking. Each material shows the ideal stress-strain curve. Figure 3.a.ii shows fCMC NF material which had the highest elasticity while withstanding the highest stress. Its stress-strain curve behaves similarly to body tissue's stress-strain curve (cite). There are four regions in this graph during tensile straining. The toe region in which the NFs have random fiber morphology that begin to re-align to remain in the lowest state of energy. The Elastic region where the NFs are fully aligned and able to retain their original shape. The plastic region where the viscosity term takes over by NFs breaking or stretching past their yield strength, permanently deforming. Each material fGel, fCMC, and fChi crosslinked through FTG, FTA, TG, and TA depicted the similar stress vs strain curves. They all follow the tensile properties of body tissue. In figure 3, FTA crosslinking is shown in comparison to non-crosslinked material as material FTA crosslinking withstood the highest stress in fCMC and fChi material.

#### *4.4.2 Maximum Stress for dry FSG NF material*

Each material fGel, fCMC, and fChi had a higher elasticity and withstood more stress when crosslinked rather than non-crosslinked. The molecular bonds formed during

crosslinking removed excess H<sub>2</sub>O leaving stronger bonds. The fCMC material had the highest maximum stress at  $0.83 \pm 0.15$ MPa with FTA crosslinking for all materials. From a T-test: two sampling, the fCMC – FTA material's stress was statistically significantly different than both fChi-FTA  $0.47 \pm 0.08$ MPa and fCMC-FTG  $0.30 \pm 0.13$ MPa material which was the highest stress withstood in fChi and fGel, figure 4. The polysaccharide CMC improved the mechanical properties of electrospun FSG NF material. Similar to others reporting cellulose having good mechanical properties (Kanikireddy et al., 2020; Pérez-Madrugal et al., 2018).

The AGA enhanced thermally crosslinking (TA) improved the yield strength of fCMC better than GTA combines with thermal crosslinking (TG). Freeze Drying (FD) for TA additionally improved the yield strength. For GTA crosslinking fCMC, FD did not make a difference in maximum yield strength, figure 4. The fChi crosslinked with TG compared to TA produced a higher yield strength without FD, fChi-TG  $0.42 \pm 0.69$ MPa. With FD fChi TA crosslinking had a slightly higher yield strength of  $0.47 \pm 0.83$ MPa but not statistically significant. For the fGel material with no polysaccharides, FTG produced the highest yield strength. Overall, Freeze Drying the FSG NF material was beneficial to increase yield strength, except for fChi-FTG. Additionally, with polysaccharides added to FSG, AGA enhanced thermally crosslinking had a higher maximum stress than GTA and thermally crosslinking. This is due to more uniform crosslinking with the monosaccharide AGA, as opposed to mainly surface crosslinking with GTA (Dechojarassri et al., 2023).

#### *4.4.2 Elasticity modulus for dry, wet, and wet degraded samples*

The FSG NF material wet mechanical properties behaved similarly to a blood vessel's mechanical properties called strain hardening. In figure 5, the fCMC material with FTA and FTG crosslinking both show two elastic moduli along the stress-strain curve. The lower elastic moduli is indicative of elastin in the body's ECM which ends halfway along the stress-strain curve (Ebrahimi, 2009; Sutherland et al., 2022). Then the next elastic modulus comes from collagen fibers being strained. As a result, the second modulus is higher in value indicating a stiffer material. The elastic moduli shown in table 3 come from the second moduli in the stress-strain curve for comparison of FSG to collagen.

For dry condition, the FTA and FTG crosslinking procedures gave the FSG NF material the best mechanical properties with an elastic modulus on the order of MPa. In literature there are several reporting's of different elastic moduli for vascular tissue (Ebrahimi, 2009; Hu et al., 2023; L'Heureux et al., 1998; Sutherland et al., 2022; Suzuki et al., 2023; Travers et al., 2016) with the main organ being blood vessels. The difference in elastic moduli varies due to multi-layers in a blood vessel (Ma et al., 2023). Additionally, various mechanical tests such as: radial, axial, and burst pressure (Camasão and Mantovani, 2021). This paper focused on a 2D, one layered material for tensile tests in dry and wet conditions. The decrease in elastic modulus for the material from dry to wet state was due to swelling of the NF in fluid. This caused the NFs to more easily rearrange and have less friction against each other becoming less stiff. The two crosslinking techniques that performed best in dry state were utilized for tensile tests of the FSG NF material in Fetal Bovine Serum (FBS) at normal body temperature.

Table 3: Elasticity moduli of fCMC, fChi, and fGel after crosslinking with FTA and FTG. The material was strained when dry, after five minutes of exposure to FBS, and after degrading in FBS for 24 hours. The crosslinking procedure FTA performed best for the dry material. For the wet material fChi became stiffer after 24hours in FBS fGel and fCel did not have significant change when wet.

| <i>Samples</i>  | <b>Modulus (kPa) in dry state</b> | <b>Modulus (kPa) in FBS after 5 min exposure</b> | <b>Modulus (kPa) in FBS after 24 h</b> |
|-----------------|-----------------------------------|--|--|
| <i>fCMC-FTA</i> | 17022.7 ± 4910.3                  | 44.0 ± 12.3                                      | 41.9 ± 10.6                            |
| <i>fCMC-FTG</i> | 12743.7 ± 2899.7                  | 57.0 ± 20.5                                      | 64.9 ± 7.6                             |
| <i>fChi-FTA</i> | 7107.1 ± 2321.0                   | 32.3 ± 5.7                                       | 17.0 ± 4.8                             |
| <i>fChi-FTG</i> | 6486.4 ± 967.4                    | 17.7 ± 5.5                                       | 12.3 ± 2.5                             |
| <i>fGel-FTA</i> | 8491.7 ± 1029                     | 15.3 ± 3.1                                       | 14.1 ± 2.7                             |
| <i>fGel-FTG</i> | 11422.4 ± 2063.3                  | 35.1 ± 7.2                                       | 33.2 ± 6.6                             |

The fCMC- and fGel-FTA material had lower elastic moduli ( $44.0 \pm 12.3$  kPa and  $15.3 \pm 3.1$  kPa) then fCMC- and fGel-FTG crosslinked. The FTG crosslinking technique caused a stiffer material due to GTA causing inter- and intra-fiber crosslinking (Dechojarassri et al., 2023). AGA enhanced thermal crosslinking (TA) only caused intra-fiber crosslinking (Dechojarassri et al., 2023; Furuike et al., 2016) as the AGA is electrospun within the NF. Intra-fiber crosslinking allowed the NFs to re-arrange more easily when stress was applied. So FTA crosslinked material was more elastic. The fChi material showed the opposite with FTG having a lower elastic modulus  $17.7 \pm 5.5$  kPa). Crosslinking with Chi and GTA caused stronger bonding then Chi and AGA enhanced thermal crosslinking.

After the FSG NF materials had degraded in FBS at 37°C for 24h, the fCMC and fGel material did not show a statistically significant difference. However, fChi material decreased in elasticity for both FTA and FTG crosslinking. During fChi precursor preparation the solvent was heated to allow supersaturation of Chi. Further heat

treatment of the material with thermal crosslinking the caused non-uniform bonding producing a lower elastic modulus for fChi material after degrading in FBS for 24h at 37°C. The polysaccharide CMC combined with FSG easily mixed with no catalyst resulting in stronger, uniform bonding.

#### 4.5 Porosity effect on mechanical properties

A vascular tissue needs to have a high surface to pore ratio for cells to seed through (Heydarkhan-Hagvall et al., 2008; Rahmati et al., 2021). All of the FSG NF material, table 4, have a high porosity ranging from  $98.1 \pm 0.02$  to  $99.2 \pm 0.2\%$ . Electrospinning is unique in that pore sizes can be increased or decreased due to amount of polymer in a solution (Hasan et al., 2014; Ma and Zhang, 1999). More polymer promotes thicker NF diameters which decreases porosity but increasing mechanical strength. The FSG NF material in table 4 have good

Table 4: Porosity of each material with various crosslinking procedures. The porosity was very similar.

| <b>Samples</b>      | <b>Porosity %</b> |
|---------------------|-------------------|
| fCMC noncrosslinked | $98.6 \pm 0.13$   |
| fCMC-FTA            | $98.8 \pm 0.03$   |
| fCMC-TA             | $98.1 \pm 0.02$   |
| fCMC-TG             | $98.3 \pm 0.13$   |
| fCMC-FTG            | $98.7 \pm 1.55$   |
| fChi noncrosslinked | $99.1 \pm 0.38$   |
| fChi-FTA            | $98.9 \pm 0.04$   |
| fChi-TA             | $98.8 \pm 0.07$   |
| fChi-FTG            | $98.8 \pm 0.02$   |
| fChi-TG             | $99.0 \pm 0.04$   |
| fGel noncrosslinked | $99.2 \pm 0.20$   |

|          |                 |
|----------|-----------------|
| fGel-FTA | $98.7 \pm 0.22$ |
| fGel-TA  | $98.8 \pm 0.04$ |
| fGel-FTG | $98.7 \pm 0.14$ |
| fGel-TG  | $99.1 \pm 0.03$ |

mechanical strength for such high porosity. To decrease porosity the FSG NF material could have been compressed for a denser material or more polymer added into the material.

#### 4 Conclusions

A Fish Skin Gelatin (FSG) nanofibrous (NF) viscoelastic material was fabricated through a high-yield process of Alternating Field Electrospinning with various post processing treatments. The post-processing treatments showed an ability to control the degradation rate of this material. With freeze drying's removal of weaker water bonds causing the material to degrade more slowly. N-acetyl-D-glucosamine (AGA) enhanced thermal crosslinking had a comparable degradation rate control to the common glutaraldehyde (GTA) vapor plus thermal crosslinking. AGA enhanced crosslinking can be substituted for GTA plus thermal crosslinking as a safer, healthier alternative. The post processing procedures for FSG NFs material that showed the highest mass retention over one week were Freeze drying with GTA plus thermal crosslinking (FTG) and freeze-drying AGA enhanced thermal crosslinking (FTA). Both crosslinking procedures for FSG NFs showed strain hardening in a physiological environment which is similar to natural body tissue. The addition of polysaccharide of carboxyl methyl cellulose salt (CMC) and chitonase (Chi) both improved the maximum stress the material was able to

withstand. However, the FSG Chi material (fChi) became almost 30% stiffer after degrading in fetal bovine serum (FBS) after 24h then when just exposed to FBS for 5min. Overall, this viscoelastic FSG NF material with and without the addition of polysaccharides can be made scale-up through AFES and shows viable properties as a vascular tissue platform.

## References

- Camasão DB, Mantovani D. The mechanical characterization of blood vessels and their substitutes in the continuous quest for physiological-relevant performances. A critical review. *Mater Today Bio* 2021;10:100106. <https://doi.org/10.1016/j.mtbio.2021.100106>.
- Chen Y, Dong X, Shafiq M, Myles G, Radacsi N, Mo X. Recent Advancements on Three-Dimensional Electrospun Nanofiber Scaffolds for Tissue Engineering. *Adv Fiber Mater* 2022;4:959–86. <https://doi.org/10.1007/s42765-022-00170-7>.
- Chiulan I, Heggset EB, Voicu ȘI, Chinga-Carrasco G. Photopolymerization of Bio-Based Polymers in a Biomedical Engineering Perspective. *Biomacromolecules* 2021;22:1795–814. <https://doi.org/10.1021/acs.biomac.0c01745>.
- Dechojarassri D, Kaneshige R, Tamura H, Furuike T. Preparation and Characterization of Crosslinked Electrospun Gelatin Fabrics via Maillard Reactions. *Materials* 2023;16:4078. <https://doi.org/10.3390/ma16114078>.
- Ebrahimi AP. Mechanical Properties of Normal and Diseased Cerebrovascular System. *J Vasc Interv Neurol* 2009;2:155–62.
- Felt O, Buri P, Gurny R. Chitosan: A Unique Polysaccharide for Drug Delivery. *Drug Dev Ind Pharm* 1998;24:979–93. <https://doi.org/10.3109/03639049809089942>.
- Furuike T, Chaochai T, Okubo T, Mori T, Tamura H. Fabrication of nonwoven fabrics consisting of gelatin nanofibers cross-linked by glutaraldehyde or N-acetyl-d-glucosamine by aqueous method. *Int J Biol Macromol* 2016;93:1530–8. <https://doi.org/10.1016/j.ijbiomac.2016.03.053>.
- Ghassemi Z, Slaughter G. Storage stability of electrospun pure gelatin stabilized with EDC/Sulfo-NHS. *Biopolymers* 2018;109:e23232. <https://doi.org/10.1002/bip.23232>.
- Gomes SR, Rodrigues G, Martins GG, Henriques CMR, Silva JC. In vitro evaluation of crosslinked electrospun fish gelatin scaffolds. *Mater Sci Eng C* 2013;33:1219–27. <https://doi.org/10.1016/j.msec.2012.12.014>.
- González-Ulloa G, Jiménez-Rosado M, Ráfii-El-Idrissi Benhnia M, Romero A, Ruiz-Mateos E, Ostos FJ, et al. Hybrid polymeric Hydrogel-based biomaterials with potential applications in regenerative medicine. *J Mol Liq* 2023;384:122224. <https://doi.org/10.1016/j.molliq.2023.122224>.
- Gungor M, Sagirli MN, Calisir MD, Selcuk S, Kilic A. Developing centrifugal spun thermally cross-linked gelatin based fibrous biomats for antibacterial wound dressing applications. *Polym Eng Sci* 2021;61:2311–22. <https://doi.org/10.1002/pen.25759>.

- Hasan A, Memic A, Annabi N, Hossain M, Paul A, Dokmeci MR, et al. Electrospun scaffolds for tissue engineering of vascular grafts. *Acta Biomater* 2014;10:11–25. <https://doi.org/10.1016/j.actbio.2013.08.022>.
- Heydarkhan-Hagvall S, Schenke-Layland K, Dhanasopon AP, Rofail F, Smith H, Wu BM, et al. Three-dimensional electrospun ECM-based hybrid scaffolds for cardiovascular tissue engineering. *Biomaterials* 2008;29:2907–14. <https://doi.org/10.1016/j.biomaterials.2008.03.034>.
- Hu G, Li G, Chen L, Hong FF. Production of novel elastic bacterial nanocellulose/polyvinyl alcohol conduits via mercerization and phase separation for small-caliber vascular grafts application. *Int J Biol Macromol* 2023;239:124221. <https://doi.org/10.1016/j.ijbiomac.2023.124221>.
- Huang T, Tu Z, Shangguan X, Sha X, Wang H, Zhang L, et al. Fish gelatin modifications: A comprehensive review. *Trends Food Sci Technol* 2019;86:260–9. <https://doi.org/10.1016/j.tifs.2019.02.048>.
- Kanikireddy V, Varaprasad K, Jayaramudu T, Karthikeyan C, Sadiku R. Carboxymethyl cellulose-based materials for infection control and wound healing: A review. *Int J Biol Macromol* 2020;164:963–75. <https://doi.org/10.1016/j.ijbiomac.2020.07.160>.
- Kennell A, MacEwen M, Armstrong M, Nicola T, Halloran B, Ambalavanan N, et al. Fish skin gelatin nanofibrous scaffolds spun using alternating field electrospinning and in-vitro tested with tdTomato mice fibroblasts. *Mater Today Commun* 2022;31:103417. <https://doi.org/10.1016/j.mtcomm.2022.103417>.
- Kovács A., Nyerges B., Izvekov V., Vibrational Analysis of N-Acetyl- $\alpha$ -D-glucosamine and  $\beta$ -D-Glucuronic Acid, *J. Phys. Chem. B* 2008, 112, 5728-5735. [doi.org/10.1021/jp710432d](https://doi.org/10.1021/jp710432d)
- Kudo S., Nakashima S., *Spectrochim. Acta A Mol. Biomol. Spectrosc.* **2020**, *241*, 118619.
- Kwak HW, Park J, Yun H, Jeon K, Kang D-W. Effect of crosslinkable sugar molecules on the physico-chemical and antioxidant properties of fish gelatin nanofibers. *Food Hydrocoll* 2021;111:106259. <https://doi.org/10.1016/j.foodhyd.2020.106259>.
- Lacy HA, Jenčová V, Lukáš D, Stanishevsky A. Alternating field electrospinning of blended fish gelatin/poly( $\epsilon$ -caprolactone) nanofibers. *Mater Lett* 2023;341:134284. <https://doi.org/10.1016/j.matlet.2023.134284>.
- L'Heureux N, Pâquet S, Labbé R, Germain L, Auger FA. A completely biological tissue-engineered human blood vessel. *FASEB J* 1998;12:47–56. <https://doi.org/10.1096/fsb2fasebj.12.1.47>.

- Lim D-J. Cross-Linking Agents for Electrospinning-Based Bone Tissue Engineering. *Int J Mol Sci* 2022;23. <https://doi.org/10.3390/ijms23105444>.
- Liu C, Yu Q, Yuan Z, Guo Q, Liao X, Han F, et al. Engineering the viscoelasticity of gelatin methacryloyl (GelMA) hydrogels via small “dynamic bridges” to regulate BMSC behaviors for osteochondral regeneration. *Bioact Mater* 2023;25:445–59. <https://doi.org/10.1016/j.bioactmat.2022.07.031>.
- Liu G, Zou F, He W, Li J, Xie Y, Ma M, et al. The controlled degradation of bacterial cellulose in simulated physiological environment by immobilization and release of cellulase. *Carbohydr Polym* 2023;314:120906. <https://doi.org/10.1016/j.carbpol.2023.120906>.
- Ma J, Li Y, Yang X, Liu K, Zhang X, Zuo X, et al. Signaling pathways in vascular function and hypertension: molecular mechanisms and therapeutic interventions. *Signal Transduct Target Ther* 2023;8:1–30. <https://doi.org/10.1038/s41392-023-01430-7>.
- Ma PX, Zhang R. Synthetic nano-scale fibrous extracellular matrix. *J Biomed Mater Res* 1999;46:60–72. [https://doi.org/10.1002/\(SICI\)1097-4636\(199907\)46:1<60::AID-JBM7>3.0.CO;2-H](https://doi.org/10.1002/(SICI)1097-4636(199907)46:1<60::AID-JBM7>3.0.CO;2-H).
- Methods of Chitosan Identification: History and Trends. *Lett Appl NanoBioScience* 2022;12:94. <https://doi.org/10.33263/LIANBS124.094>.
- Mo H, Qiu J, Yang C, Zang L, Sakai E, Chen J. Porous biochar/chitosan composites for high performance cellulase immobilization by glutaraldehyde. *Enzyme Microb Technol* 2020;138:109561. <https://doi.org/10.1016/j.enzmictec.2020.109561>.
- Noble L, Gray AI, Sadiq L, Uchegbu IF. A non-covalently cross-linked chitosan based hydrogel. *Int J Pharm* 1999;192:173–82. [https://doi.org/10.1016/S0378-5173\(99\)00306-3](https://doi.org/10.1016/S0378-5173(99)00306-3).
- Pellá MCG, Lima-Tenório MK, Tenório-Neto ET, Guilherme MR, Muniz EC, Rubira AF. Chitosan-based hydrogels: From preparation to biomedical applications. *Carbohydr Polym* 2018;196:233–45. <https://doi.org/10.1016/j.carbpol.2018.05.033>.
- Pérez-Madrugal MM, Edo MG, Saborío MG, Estrany F, Alemán C. Pastes and hydrogels from carboxymethyl cellulose sodium salt as supporting electrolyte of solid electrochemical supercapacitors. *Carbohydr Polym* 2018;200:456–67. <https://doi.org/10.1016/j.carbpol.2018.08.009>.
- Persano L, Camposeo A, Tekmen C, Pisignano D. Industrial Upscaling of Electrospinning and Applications of Polymer Nanofibers: A Review. *Macromol Mater Eng* 2013;298:504–20. <https://doi.org/10.1002/mame.201200290>.

- Pokorny P, Kostakova E, Sanetnik F, Mikes P, Chvojka J, Kalous T, et al. Effective AC needleless and collectorless electrospinning for yarn production. *Phys Chem Chem Phys* 2014;16:26816–22. <https://doi.org/10.1039/C4CP04346D>.
- Polyak F., Reich G., Infrared spectroscopic study of the coil-helix transition of highly concentrated gelatin formulations, *Eur. J. Pharm. Biopharm.* 140 (2019) 11–19. <https://doi.org/10.1016/j.ejpb.2019.04.010>
- Powell-Wiley TM, Poirier P, Burke LE, Després J-P, Gordon-Larsen P, Lavie CJ, et al. Obesity and Cardiovascular Disease: A Scientific Statement From the American Heart Association. *Circulation* 2021;143:e984–1010. <https://doi.org/10.1161/CIR.0000000000000973>.
- Prystupa D.A., Donald A.M., Infrared study of gelatin conformations in the gel and sol states, *Polymer Gels and Networks* 4 (1996) 87-110
- Rahmati M, Mills DK, Urbanska AM, Saeb MR, Venugopal JR, Ramakrishna S, et al. Electrospinning for tissue engineering applications. *Prog Mater Sci* 2021;117:100721. <https://doi.org/10.1016/j.pmatsci.2020.100721>.
- Skopinska-Wisniewska J, Tuszynska M, Olewnik-Kruszkowska E. Comparative study of gelatin hydrogels modified by various cross-linking agents. *Materials* 2021;14:1–17. <https://doi.org/10.3390/ma14020396>.
- Smith IO, Liu XH, Smith LA, Ma PX. Nanostructured polymer scaffolds for tissue engineering and regenerative medicine. *WIREs Nanomedicine Nanobiotechnology* 2009;1:226–36. <https://doi.org/10.1002/wnan.26>.
- Soliman AM, Teoh SL, Das S. Fish Gelatin: Current Nutritional, Medicinal, Tissue Repair Applications, and as a Carrier of Drug Delivery. *Curr Pharm Des* 2022;28:1019–30. <https://doi.org/10.2174/1381612828666220128103725>.
- Sutherland DW, McEleney A, de Almeida M, Kajimoto M, Ventura G, Isenberg BC, et al. Characterization of main pulmonary artery and valve annulus region of piglets using echocardiography, uniaxial tensile testing, and a novel non-destructive technique. *Front Cardiovasc Med* 2022;9:884116. <https://doi.org/10.3389/fcvm.2022.884116>.
- Suzuki S, Mori S, Iwai-Takano M, Arakawa M, Kanai H. Internal pressure dependence on viscoelasticity of arterial wall by ultrasonic measurement. *Jpn J Appl Phys* 2023;62. <https://doi.org/10.35848/1347-4065/acbf5d>.
- Travers JG, Kamal FA, Robbins J, Yutzey KE, Blaxall BC. Cardiac Fibrosis. *Circ Res* 2016;118:1021–40. <https://doi.org/10.1161/CIRCRESAHA.115.306565>.
- Warner EL, Norton IT, Mills TB. Comparing the viscoelastic properties of gelatin and different concentrations of kappa-carrageenan mixtures for additive

manufacturing applications. *J Food Eng* 2019;246:58–66.  
<https://doi.org/10.1016/j.jfoodeng.2018.10.033>.

Zhang Y., Ouyang H, Lim C.T., Ramakrishna S., Huang Z.M. *J. Biomed. Mater. Res. B.* 2005, 72, 156-165.

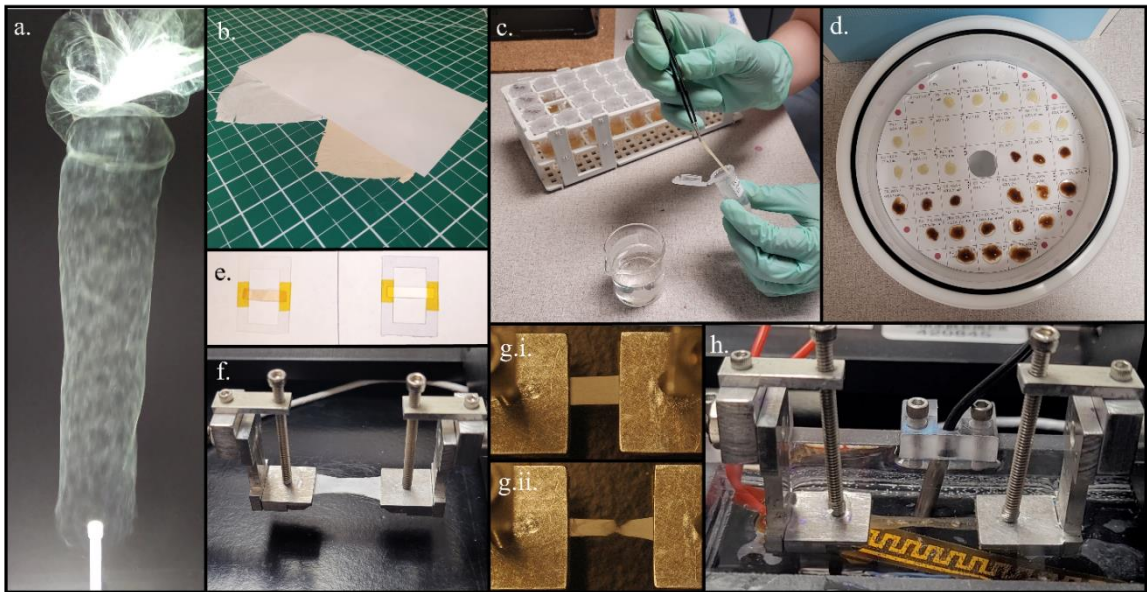


Figure 1: FSG NFs produced by AFES then crosslinked various ways to mimic a biomaterial's mechanical properties. (a) is FSG NFs being fabricated with a cylindrical shape. (b) is the fGel material thermally crosslinked with and with out AGA enhancement. AGA causes the color change in the fGel NFs material due to the maillard during thermal crosslinking. (c) is fGel material prepared for a degradation test. (d) shows the fGel material after the degradation test being dried in a vacuum. (e) is fGel material cut and placed into frames. The frames prevent the NFs from folding while in SBF. (f) is mechanically testing dry fGel material. (g) is before straining and after breaking the dry fGel material. (h) is fGel material being strained in FBS at 37° C.

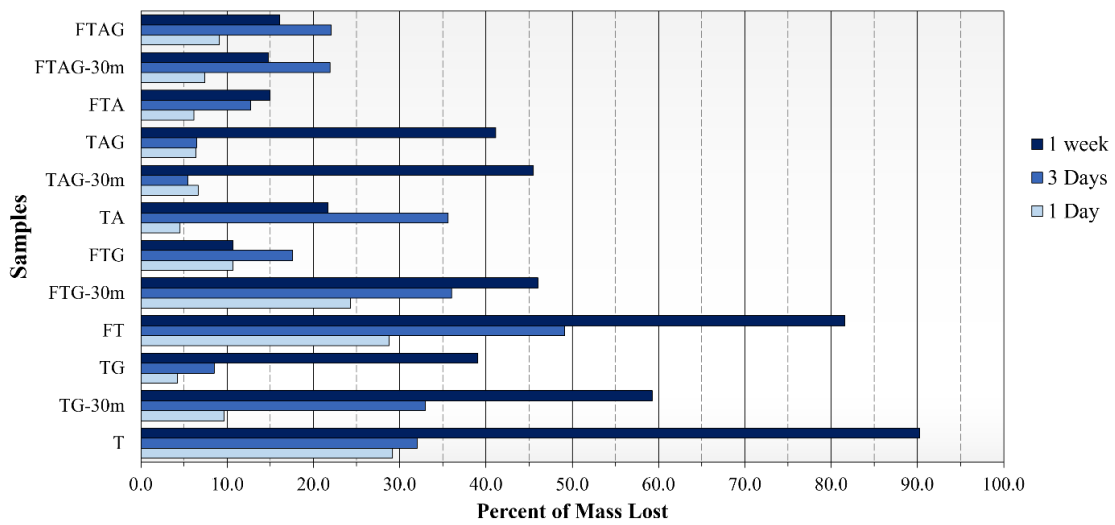
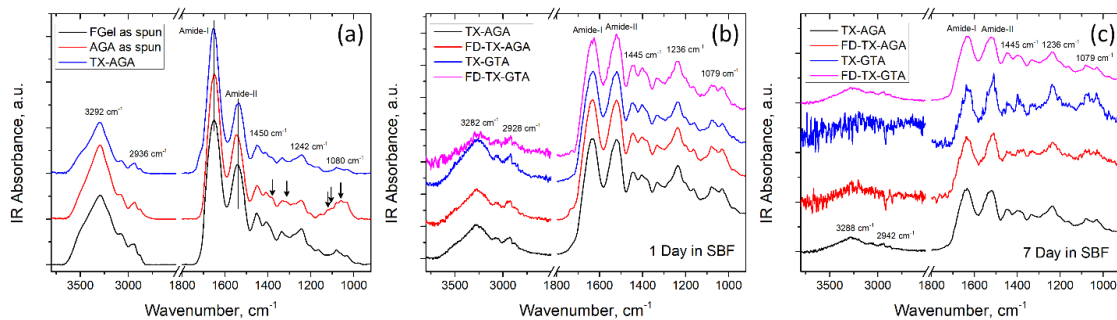


Figure 2: Mass loss of fGel material with various crosslinking methods. The fGel-FTG and fGel-FTA degraded the least losing 10.7% (FTG) and 15.0% (FTA) of their original mass after a week period. Comparatively the fGel-T material lost the most mass over the week period. If T crosslinking was combined with another post-processing method the material retained more mass.



**Figure 3.** FTIR absorption spectra of representative fGel-based nanofibrous materials after (a) electrospinning and thermal crosslinking; (b) after 1 day and (c) 7 days of degradation in SBF.

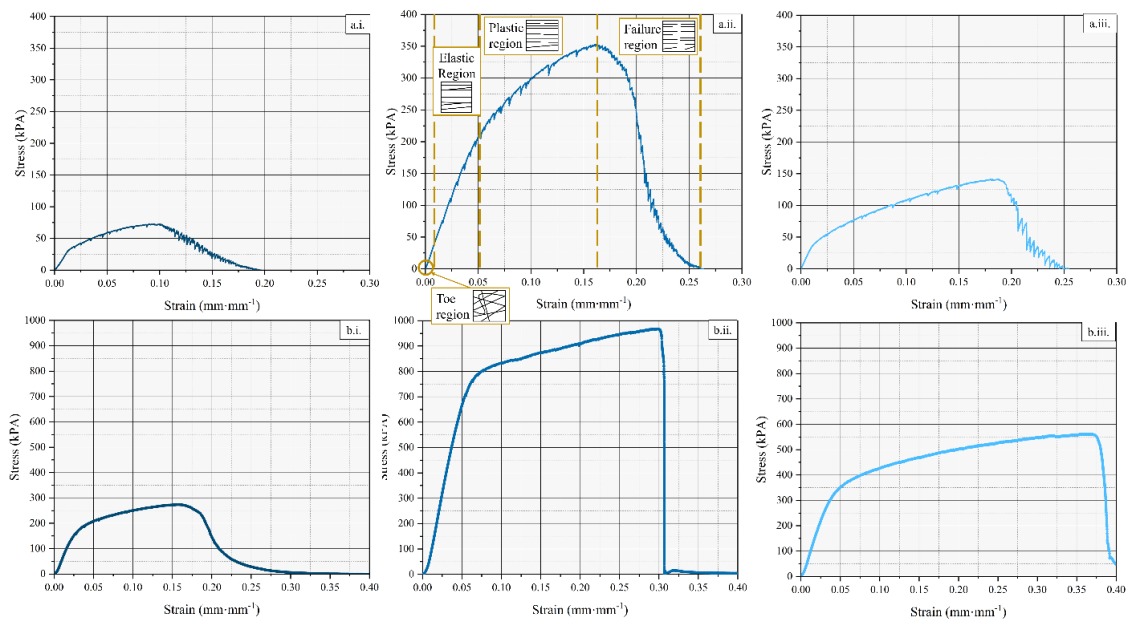


Figure 4: Stress vs. Strain curves of fGel, fCMC, and fChi materials. (a.i.) shows non-crosslinked Gel material's mechanical behavior. (a.ii.) shows non-crosslinked fCMC material's mechanical behavior, additionally, with the four regions of a stress vs. strain curve. fCMC reaches the highest stress level. (a.iii.) shows non-crosslinked fChi material. (b.i.) shows fGel-FTA crosslinked material's mechanical behavior while dry. (b.ii.) shows fCMC-FTA crosslinked material's mechanical behavior while dry. (b.iii.) shows fChi-FTA crosslinked materials mechanical behavior while dry.

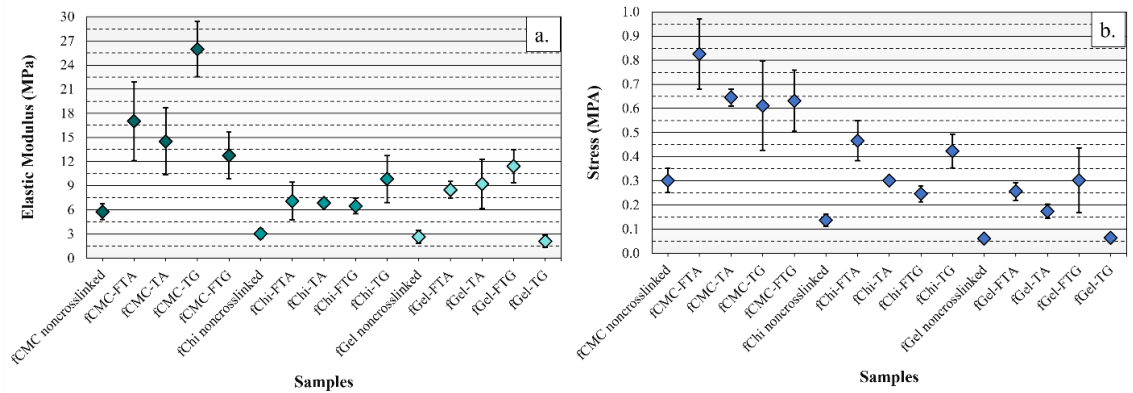


Figure 5: tensile tests of various gelatin materials crosslinked different ways. (a) materials were strained laterally to obtain their elasticity modulus and yield strength. The fCMC material regardless of crosslinking procedure had the highest elasticity modulus. (b) is the maximum stress withstood by the FSG material until breakage. The fCMC material withstood the highest stress.

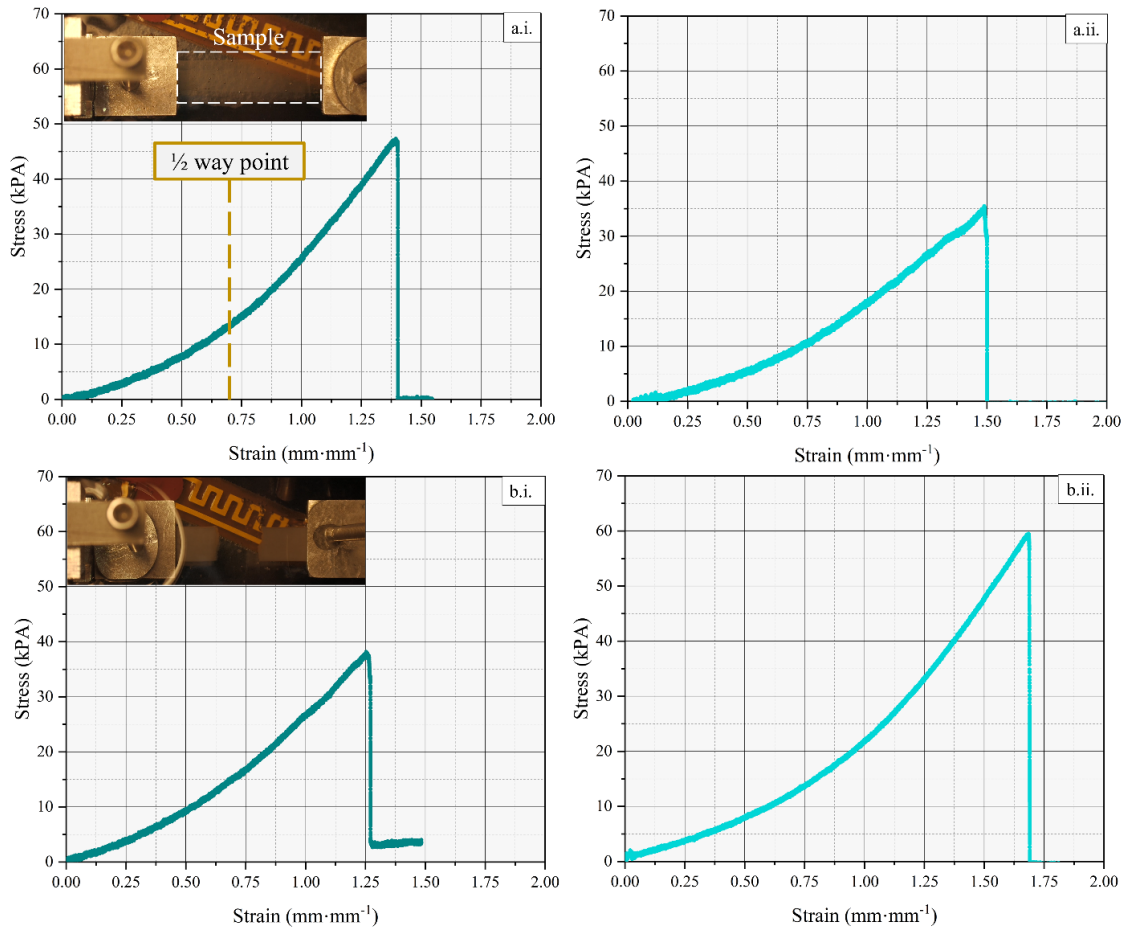


Figure 6: fCMC material mechanically tested under normal body condition. The material is in FBS that has a temperature of 37°C. (a.i.) is fCMC-FTA crosslinked and (b.i.) is fCMC-FTG crosslinked both have been just submersed in SBF for 5min. (a.ii.) is fCMC-FTA crosslinked and (b.ii.) is fCMC-FTG crosslinked both have been left in FBS at normal body temperature for twenty-four hours. Some materials never broke as they were to elastic. The elastic modulus was taken from the second elastic region.

## CONCLUSIONS

An innovative biomaterial platform of fish skin gelatin (FSG) with and without polymer additives was tissue engineered (TE) with alternating current electrospinning for tissue healing. This nanofibrous (NF) FSG material has a higher yield than any other reported TE gelatin NFs with a production rate of 12.6g/h. Confirmation of the NF FSG extracellular matrix (ECM) biocompatible transpired with cell proliferation of a novel cell line, tdTomato mice fibroblasts. The usage of tdTomato mice fibroblasts additionally lowered cost of cell staining compared to the commonly used green fluorescent protein staining while allowing live imaging of the FSG ECM. Post processing treatments on this NF FSG viscoelastic biomaterial, enabled a unique property of a controllable degradation rate. For fast wound healing thermal crosslinking of this biomaterial is recommended while for longer wound healing post processing of freeze drying with N-Acetyl-D-Glucosamine enhanced thermal crosslinking (FTA) is recommended as FSG NF-FTA biomaterial has 85% mass retention after one week in a physiological environment. FTA produces similar results, is a safer than, and lowers cost treatment of a material as opposed to the commonly used glutaraldehyde vapor crosslinking. After post processing the biomaterial, the viscoelastic properties of the FSG alone mimicked natural body's tissue of strain hardening during mechanical testing. For natural body tissue both collagen and elastin fibers are required. Affectively, this nanofibrous fish skin gelatin material with and without additions of polysaccharides shows promise as an innovative

biomaterial platform as it is biocompatible, bioactive, biomechanically sound, and mass-producible.

## LIST OF REFERENCES

- [1] Vacanti JP, Morse MA, Saltzman WM, Domb AJ, Perez-Atayde A, Langer R. Selective cell transplantation using bioabsorbable artificial polymers as matrices. *J Pediatr Surg* 1988;23:3–9. [https://doi.org/10.1016/S0022-3468\(88\)80529-3](https://doi.org/10.1016/S0022-3468(88)80529-3).
- [2] Eldeeb AE, Salah S, Elkasabgy NA. Biomaterials for Tissue Engineering Applications and Current Updates in the Field: A Comprehensive Review. *AAPS PharmSciTech* 2022;23:267. <https://doi.org/10.1208/s12249-022-02419-1>.
- [3] Matthews JA, Wnek GE, Simpson DG, Bowlin GL. Electrospinning of collagen nanofibers. *Biomacromolecules* 2002;3:232–8. <https://doi.org/10.1021/bm015533u>.
- [4] Shin M, Ishii O, Sueda T, Vacanti JP. Contractile cardiac grafts using a novel nanofibrous mesh. *Biomaterials* 2004;25:3717–23. <https://doi.org/10.1016/j.biomaterials.2003.10.055>.
- [5] Xu C. Aligned biodegradable nanofibrous structure: a potential scaffold for blood vessel engineering. *Biomaterials* 2004;25:877–86. [https://doi.org/10.1016/S0142-9612\(03\)00593-3](https://doi.org/10.1016/S0142-9612(03)00593-3).
- [6] Chen P-H, Liao H-C, Hsu S-H, Chen R-S, Wu M-C, Yang Y-F, et al. A novel polyurethane/cellulose fibrous scaffold for cardiac tissue engineering. *RSC Adv* 2015;5:6932–9. <https://doi.org/10.1039/C4RA12486C>.
- [7] Micropatterning of three-dimensional electrospun polyurethane vascular grafts. - PubMed - NCBI n.d. <https://www.ncbi.nlm.nih.gov/pubmed/20601235> (accessed December 4, 2019).
- [8] Songchotikunpan P, Tattiyakul J, Supaphol P. Extraction and electrospinning of gelatin from fish skin. *Int J Biol Macromol* 2008;42:247–55. <https://doi.org/10.1016/j.ijbiomac.2007.11.005>.
- [9] Boland E D. Electrospinning collagen and elastin: preliminary vascular tissue engineering. *Front Biosci* 2004;9:1422. <https://doi.org/10.2741/1313>.
- [10] Reddy MSB, Ponnamma D, Choudhary R, Sadasivuni KK. A Comparative Review of Natural and Synthetic Biopolymer Composite Scaffolds. *Polymers* 2021;13:1105. <https://doi.org/10.3390/polym13071105>.
- [11] Advances in tissue engineering. *J Pediatr Surg* 2016;51:8–12. <https://doi.org/10.1016/j.jpedsurg.2015.10.022>.

- [12] Tran HA, Hoang TT, Maraldo A, Do TN, Kaplan DL, Lim KS, et al. Emerging silk fibroin materials and their applications: New functionality arising from innovations in silk crosslinking. *Mater Today* 2023;65:244–59. <https://doi.org/10.1016/j.mattod.2023.03.027>.
- [13] Dardano P, Caliò A, Di Palma V, Bevilacqua MF, Di Matteo A, De Stefano L. A Photolithographic Approach to Polymeric Microneedles Array Fabrication. *Materials* 2015;8:8661–73. <https://doi.org/10.3390/ma8125484>.
- [14] Karageorgiou V, Kaplan D. Porosity of 3D biomaterial scaffolds and osteogenesis. *Biomaterials* 2005;26:5474–91. <https://doi.org/10.1016/j.biomaterials.2005.02.002>.
- [15] Jhon MS, Andrade JD. Water and hydrogels. *J Biomed Mater Res* 1973;7:509–22. <https://doi.org/10.1002/jbm.820070604>.
- [16] Chaudhari AA, Vig K, Baganizi DR, Sahu R, Dixit S, Dennis V, et al. Future prospects for scaffolding methods and biomaterials in skin tissue engineering: A review. *Int J Mol Sci* 2016;17. <https://doi.org/10.3390/ijms17121974>.
- [17] Lee JW, Kim JY, Cho D-W. Solid Free-form Fabrication Technology and Its Application to Bone Tissue Engineering. *Int J Stem Cells* 2010;3:85–95.
- [18] Karki S, Gohain MB, Yadav D, Ingole PG. Nanocomposite and bio-nanocomposite polymeric materials/membranes development in energy and medical sector: A review. *Int J Biol Macromol* 2021;193:2121–39. <https://doi.org/10.1016/j.ijbiomac.2021.11.044>.
- [19] Zhang S. Fabrication of novel biomaterials through molecular self-assembly. *Nat Biotechnol* 2003;21:1171–8. <https://doi.org/10.1038/nbt874>.
- [20] Ariga K, Hill JP, Lee MV, Vinu A, Charvet R, Acharya S. Challenges and breakthroughs in recent research on self-assembly. *Sci Technol Adv Mater* 2008;9:014109. <https://doi.org/10.1088/1468-6996/9/1/014109>.
- [21] Turali-Emre ES, Emre AE, Vecchio DA, Kadiyala U, VanEpps JS, Kotov NA. Self-Organization of Iron Sulfide Nanoparticles into Complex Multicompartment Supraparticles. *Adv Mater* 2023;35:2211244. <https://doi.org/10.1002/adma.202211244>.
- [22] Bhardwaj N, Kundu SC. Electrospinning: A fascinating fiber fabrication technique. *Biotechnol Adv* 2010;28:325–47. <https://doi.org/10.1016/j.biotechadv.2010.01.004>.
- [23] Beishenaliev A, Lim SS, Tshai KY, Khiew PS, Moh'd Sghayyar HN, Loh H-S. Fabrication and preliminary in vitro evaluation of ultraviolet-crosslinked electrospun fish scale gelatin nanofibrous scaffolds. *J Mater Sci Mater Med* 2019;30:62. <https://doi.org/10.1007/s10856-019-6264-4>.

- [24] Campiglio CE, Negrini NC, Farè S, Draghi L. Cross-linking strategies for electrospun gelatin scaffolds. *Materials* 2019;12. <https://doi.org/10.3390/ma12152476>.
- [25] Gao X, Han S, Zhang R, Liu G, Wu J. Progress in electrospun composite nanofibers: composition, performance and applications for tissue engineering. *J Mater Chem B* 2019;7:7075–89. <https://doi.org/10.1039/C9TB01730E>.
- [26] Liu S, Yu J-M, Gan Y-C, Qiu X-Z, Gao Z-C, Wang H, et al. Biomimetic natural biomaterials for tissue engineering and regenerative medicine: new biosynthesis methods, recent advances, and emerging applications. *Mil Med Res* 2023;10. <https://doi.org/10.1186/s40779-023-00448-w>.
- [27] Rahmati M, Mills DK, Urbanska AM, Saeb MR, Venugopal JR, Ramakrishna S, et al. Electrospinning for tissue engineering applications. *Prog Mater Sci* 2021;117:100721. <https://doi.org/10.1016/j.pmatsci.2020.100721>.
- [28] Huang T, Tu Z, Shangguan X, Sha X, Wang H, Zhang L, et al. Fish gelatin modifications: A comprehensive review. *Trends Food Sci Technol* 2019;86:260–9. <https://doi.org/10.1016/j.tifs.2019.02.048>.
- [29] Karim AA, Bhat R. Fish gelatin: properties, challenges, and prospects as an alternative to mammalian gelatins. *Food Hydrocoll* 2009;23:563–76. <https://doi.org/10.1016/j.foodhyd.2008.07.002>.
- [30] Kwak HW, Shin M, Lee JY, Yun H, Song DW, Yang Y, et al. Fabrication of an ultrafine fish gelatin nanofibrous web from an aqueous solution by electrospinning. *Int J Biol Macromol* 2017;102:1092–103. <https://doi.org/10.1016/j.ijbiomac.2017.04.087>.
- [31] Kanikireddy V, Varaprasad K, Jayaramudu T, Karthikeyan C, Sadiku R. Carboxymethyl cellulose-based materials for infection control and wound healing: A review. *Int J Biol Macromol* 2020;164:963–75. <https://doi.org/10.1016/j.ijbiomac.2020.07.160>.
- [32] Warner EL, Norton IT, Mills TB. Comparing the viscoelastic properties of gelatin and different concentrations of kappa-carrageenan mixtures for additive manufacturing applications. *J Food Eng* 2019;246:58–66. <https://doi.org/10.1016/j.jfoodeng.2018.10.033>.
- [33] Silver FH, Freeman JW, DeVore D. Viscoelastic properties of human skin and processed dermis. *Skin Res Technol Off J Int Soc Bioeng Skin ISBS Int Soc Digit Imaging Skin ISDIS Int Soc Skin Imaging ISSI* 2001;7:18–23. <https://doi.org/10.1034/j.1600-0846.2001.007001018.x>.
- [34] Kennell A, MacEwen M, Armstrong M, Nicola T, Halloran B, Ambalavanan N, et al. Fish skin gelatin nanofibrous scaffolds spun using alternating field

- electrospinning and in-vitro tested with tdTomato mice fibroblasts. *Mater Today Commun* 2022;31:103417. <https://doi.org/10.1016/j.mtcomm.2022.103417>.
- [35] Chen Y, Dong X, Shafiq M, Myles G, Radacsi N, Mo X. Recent Advancements on Three-Dimensional Electrospun Nanofiber Scaffolds for Tissue Engineering. *Adv Fiber Mater* 2022;4:959–86. <https://doi.org/10.1007/s42765-022-00170-7>.